and centrifuged at 300 *g* for 10 min, and the level of serum tartrate-resistant acid phosphatase (TRAP) 5b was measured using a mouse TRAP assay kit (SB-TR10; Immunodiagnostic Systems).

Measurements of the length and weight of femora. The femora were isolated from six to seven mice that were treated with vehicle or STZ, and the length and weight were measured.

Immunofluorescence staining for bone marrow sections. Mice were anesthetized with pentobarbital and perfused with 4% paraformaldehyde in phosphate buffer. Isolated bones were decalcified with decalcifying solution B (041–22031; WAKO), and cryostat-cut sections were prepared using adhesive film (14). Sections were blocked with 2% goat serum and incubated in rabbit anti-mouse OPN (ab8448; Abcam, Cambridge, UK) and PE-conjugated rat anti-mouse CD150 antibodies (115904; BioLegend) or sheep anti-mouse CD150 (AF4330; R&D Systems), a maker of LT-HSC (35), rat anti-mouse Tie2 (124002; BioLegend), and Pacific Blue conjugated anti-mouse lineage cocktail (133310; BioLegend) and were further incubated in Texas Red-labeled goat anti-rabbit IgG (TI-1000; Vector Laboratories), Cy3 donkey anti-sheep IgG (713–165-003; Jackson Laboratories), Alexa Fluor 647 goat anti-rat IgG (112–605-003; Jackson Laboratories), and Alexa Fluor 488 goat anti-rabbit IgG (711–544-152; Jackson Laboratories) as a secondary antibody.

Immunofluorescence staining of cultured cells. A morphological analysis of coculture cells labeled with different color of fluorescence was performed. Isolated LT-HSCs were incubated at 37°C for 1 h with the culture medium containing Qtracker 525 (Invitrogen) and then were cocultured with isolated osteoblastic niche cells at 37°C in 5%CO_2-air for 1 wk. On *day 7*, the cocultured cells were fixed with 4% paraformaldehyde in PBS, incubated with 2% BSA in PBS and stained with anti-OPN (1:50; Immuno-Biological Laboratories) in PBS containing 0.25% Triton X-100. Anti-rabbit IgG-conjugated Cy5 (1:500; ab6564; Abcam) was used as a secondary antibody. Nuclei were stained with DAPI. Fluorescence images were obtained under a confocal laser microscope (A1; Nikon, Tokyo, Japan).

Quantitative RT-PCR analysis. To examine the mRNA expression of various targets, total RNA was extracted using the RNeasy Plus Micro Kit (Qiagen), and cDNA was synthesized using the SuperScript First-Strand Synthesis System for RT-PCR (Invitrogen, Grand Island, NY). Quantitative RT-PCR for N-cadherin, β-catenin, β_1-integrin, Tie2, CXCR4, Frizzled (Fzd) receptor4, Fzd7, lipoprotein receptor-related protein 5 (LRP5), LRP6, thrombopoietin receptor (MPL), Ang-1, CXCL12, wingless-type MMTV integration site family, member 10b (Wnt10b), dickkopf-1 (Dkk1), and TPO was performed on the ABI prism 7500 Sequence Detection System (Applied Biosystems; Foster City, CA) with Power SYBR GREEN PCR Master Mix (4367659; Applied Biosystems). The relative mRNA expression was quantified by the $^{2-}\Delta C_T$ method. The primer sequences are shown in the Table 1.

IBM-BMT. To evaluate the interaction of LT-HSCs and osteoblastic niche cells in vivo, OPN^+ cells and OPN^- cells, in which LT-HSCs were included, were transplanted into bone marrow as follows: OPN^+ and OPN^- cells were sorted from the femora and tibiae of vehicle- or STZ-injected mice by MACS. Mice were irradiated (10 Gy) and transplanted with the mixture of 2×10^6 OPN^+ and 1.5×10^4 OPN^- cells derived from either diabetic or nondiabetic mice via IBM-BMT 1 day

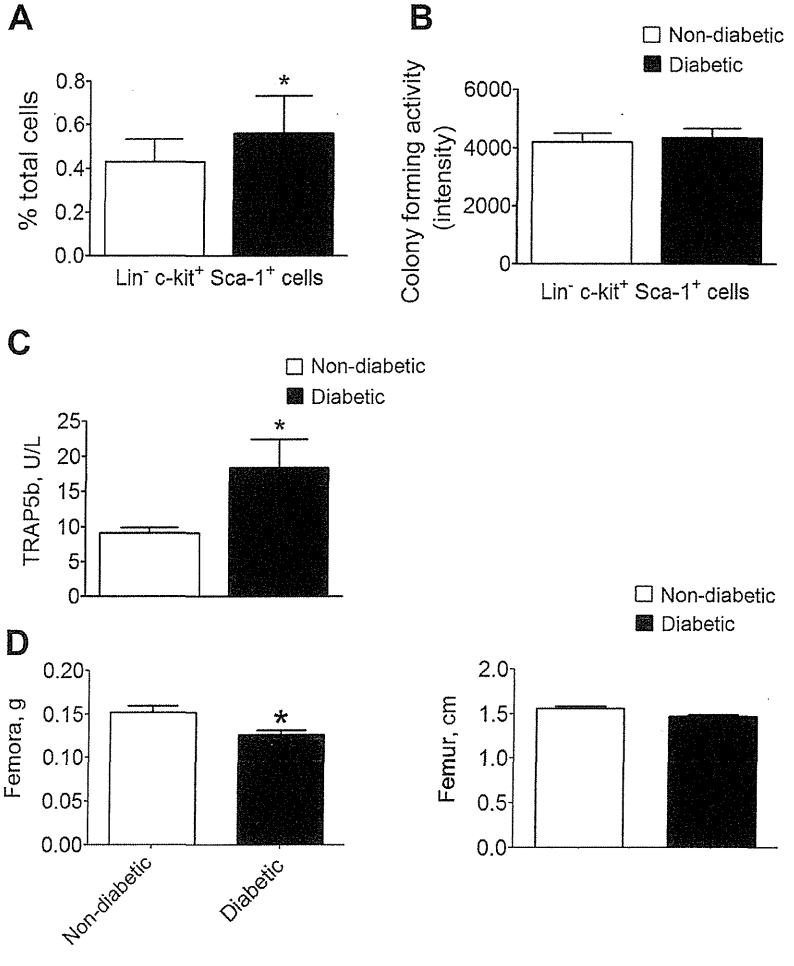

Fig. 2. Activity of Lin^-, Sca-1^+, and c-kit^+ (LSK) cells. *A*: frequency of LSK cells in mononuclear cells as determined by FACS. *B*: HSC colony-forming activity. *C*: TRAP5b activity. *D*: weight of femora and length of the femur. Values are the means ± SD for $n = 4-6$ mice. $^*P < 0.05$, compared with nondiabetic mice.

after the irradiation according to a previously study (16). One week after the bone marrow transplantation, LT-HSCs were sorted by FACS as described above, and the mRNA expression of Tie2 was examined.

Statistical analysis. Differences between groups were determined using a two-tailed Student's *t*-test and one-way ANOVA, followed by a Tukey's multiple comparison test. Differences were considered significant for values of $P < 0.05$.

RESULTS

Frequency of osteoblastic niche cells, LT-HSCs, ST-HSCs, and MPPs in diabetic and nondiabetic mouse bone marrow. The percentages of osteoblastic niche cells, LT-HSCs, ST-HSCs, and MPPs in Lin$^-$ bone marrow cells were compared, and the osteoblastic niche cells and LT-HSCs were both shown

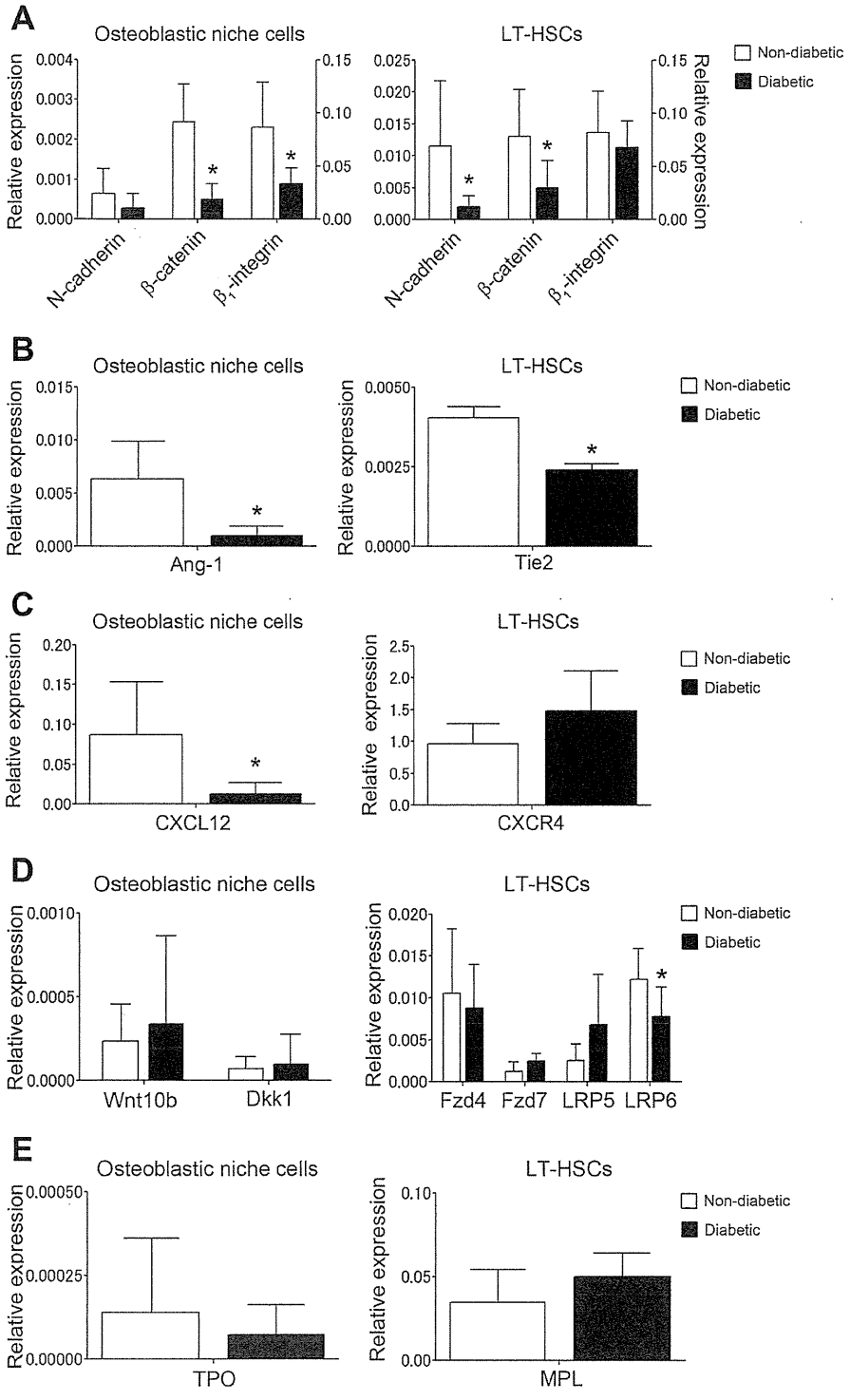

Fig. 3. Comparison of the expression levels of various molecules. *A*: expression of N-cadherin (*left axis*), β-catenin (*middle axis*), and β_1-integrin (*right axis*) on osteoblastic niche cells and LT-HSCs. *B*: expression of angiopoietin-1 (Ang-1) and Tie2. *C*: expression of CXCL12 and CXCR4. *D*: expression of proteins related to Wnt/β-catenin signaling pathways. *E*: expression of thrombopoietin (TPO) and thrombopoietin receptor (MPL). Values are the means ± SD for $n = 6-8$ mice. *$P <$ 0.05, compared with nondiabetic mice.

to be significantly reduced, while ST-HSCs and MPPs were significantly increased in diabetic mice compared with nondiabetic mice (Fig. 1*B*).

Localization of osteoblastic niche cells and LT-HSCs in diabetic and nondiabetic mouse bone marrow. The in vivo localization of osteoblastic niche cells and LT-HSCs in the bone marrow of diabetic and nondiabetic mice was examined by immunofluorescence staining (Fig. 1*C*). OPN$^+$ osteoblastic niche cells were located at the endosteum in both diabetic and nondiabetic mice (green color, arrows), and CD150-positive LT-HSCs were located adjacent to osteoblastic niche cells (red color, arrowheads).

Functional abnormalities in the HSCs from diabetic mice. To compare the hematopoiesis differentiation potentials of HSCs between diabetic and nondiabetic mice, we performed colony-forming assays on LSK cells. The number of LSK cells from the diabetic mice was significantly increased compared with that in the nondiabetic mice; however, the intensity of colony formation of differentiated cells, including neutrophil, macrophage, eosinophil, erythrocyte, and megakaryocyte from LSK cells induced by SCF, IL-3, GM-CSF, and Ep was not significantly different between diabetic and nondiabetic mice (Fig. 2, *A* and *B*). The activity of osteoclasts derived from hematopoietic progenitors was also compared between the

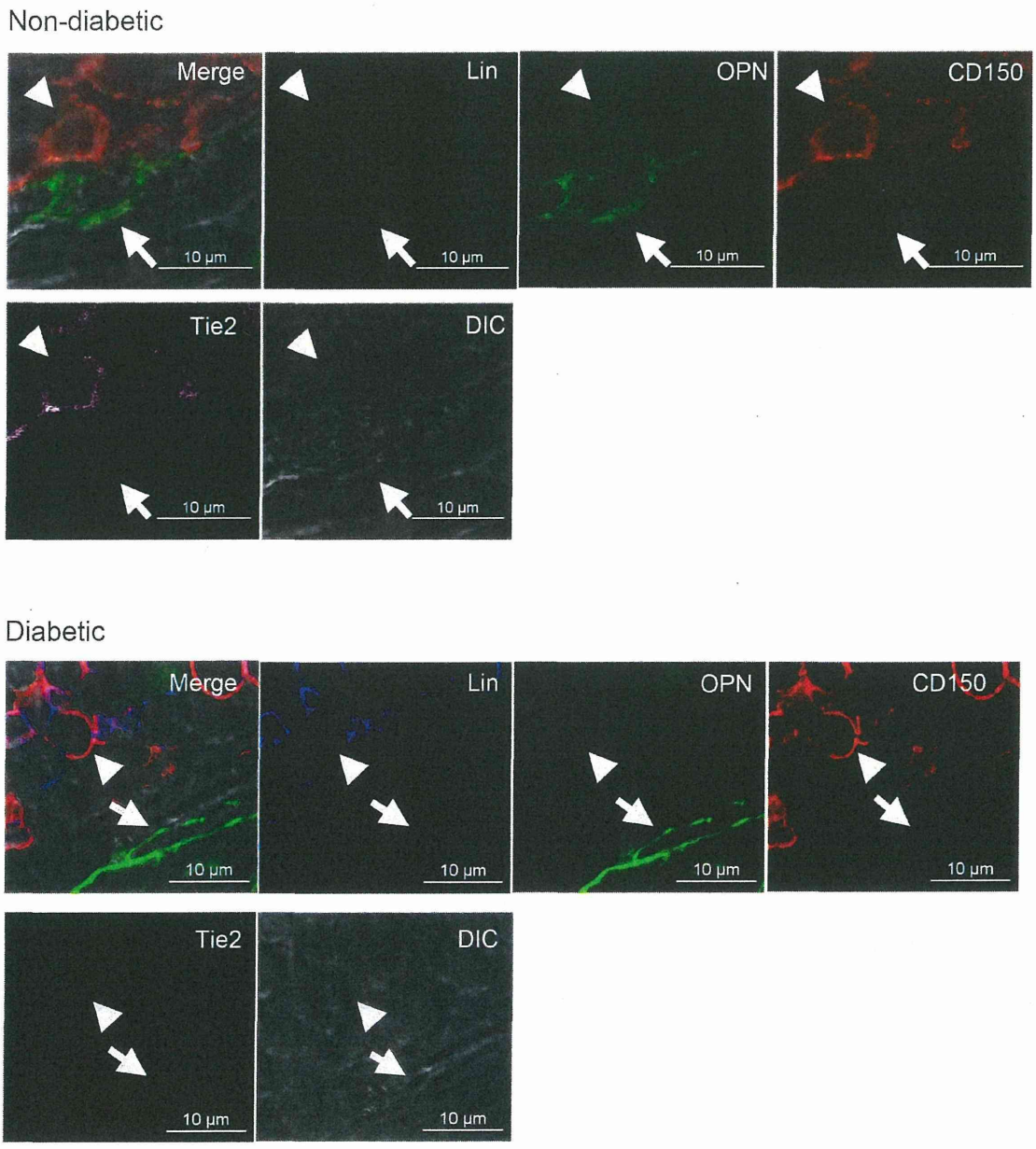

Fig. 4. Immunofluorescence staining of OPN$^+$ (green) osteoblastic niche cell (arrow) and CD150$^+$ (red) LT-HSCs (arrowhead). Lin$^-$ CD150$^+$ LT-HSC is stained with Tie 2 (pink) in nondiabetic mice; however, the intensity of Tie 2 immunoreactivity is dramatically decreased in diabetic mice.

diabetic and nondiabetic mice. TRAP5b, indicating the bone resorption activity of osteoclasts, was significantly increased in diabetic mice compared with nondiabetic mice (Fig. 2*C*). The length of the femur was not significantly different between diabetic and nondiabetic mice; however, the weight of the femora of diabetic mice was lower than that of the nondiabetic mice (Fig. 2*D*).

Expression of osteoblastic niche cell- and LT-HSC-related molecules in diabetic and nondiabetic mouse bone marrow. The expression of cell adhesion molecules such as N-cadherin, β-catenin, and β_1-integrin on isolated osteoblastic niche cells and LT-HSCs from diabetic mice was compared with that from nondiabetic mice. The expression of β-catenin and β_1-integrin on isolated osteoblastic niche cells was significantly reduced in diabetic mice, but the expression of N-cadherin was unchanged (Fig. 3*A*). Diabetic mice showed significantly reduced N-cadherin and β-catenin expression on LT-HSCs compared with nondiabetic mice, while the expression of β_1-integrin on LT-HSCs was unchanged (Fig. 3*A*). The Ang-1 expression on the osteoblastic niche cells from diabetic mice was also significantly reduced compared with that from nondiabetic mice, and the expression of the Ang-1 ligand, Tie2, on LT-HSCs was also significantly reduced in diabetic mice (Fig. 3*B*). The CXCL12 expression on osteoblastic niche cells was significantly reduced in diabetic mice, but the expression of its receptor, CXCR4, was unchanged on LT-HSCs (Fig. 3*C*). In terms of the Wnt/β-catenin signaling pathways, neither the Wnt 10b expression on osteoblastic niche cells nor the expression of receptors for Wnt family proteins, such as Fzd4, Fzd7, and LRP5, on LT-HSCs was changed; however, the LRP6 expression on LT-HSCs was reduced in diabetic mice (Fig. 3*D*). The Dkk1 expression was the same on osteoblastic niche cells from both diabetic and nondiabetic mice (Fig. 3*D*), as was the expression of TPO on osteoblastic niche cells, and the expression of its receptor, MPL, on LT-HSCs (Fig. 3*E*). In the immunohistochemical analysis for Tie 2 expression, the intensity of $Tie2^+$ immunoreactivity was dramatically decreased on Lin^- CD 150^+ LT-HSC cells in diabetic mice compared with nondiabetic mice (Fig. 4). A summary of these results is shown in Fig. 5.

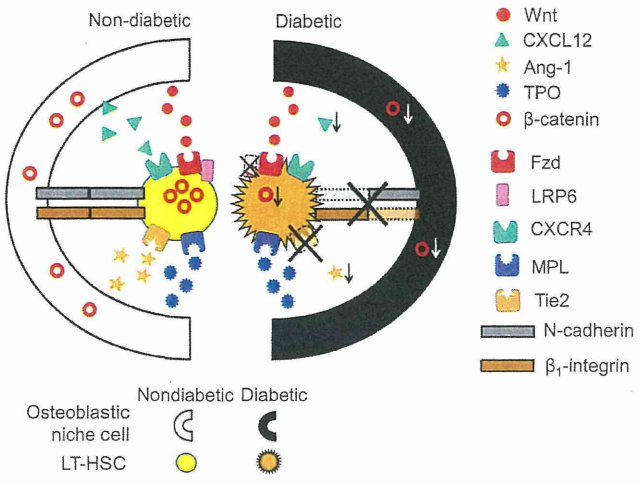

Fig. 5. Summary of the expression of molecules on osteoblastic niche cells and LT-HSCs derived from diabetic and nondiabetic mice.

In vitro coculture of osteoblastic niche cells and LT-HSCs to mimic the bone marrow microenvironment in diabetic and nondiabetic mice. We performed in vitro coculture experiments using LT-HSCs and osteoblastic niche cells derived from diabetic and nondiabetic mice. We used the 450-mg/dl (25 mM) glucose concentration as the high-glucose medium and 100-mg/dl (5.6-mM) concentration as the normal glucose medium because in the present study the blood glucose levels in diabetic and nondiabetic mice were 730.9 ± 135.6 and 167.25 ± 42.4 mg/dl, respectively (n = 15). In previous in vitro study, 5.5 and 33 mM were used as the normal and high-glucose media, and 27 mM glucose concentration was used to evaluate the effects of glucose on transplanted β-cells as an in vitro diabetic condition (20, 32). After 7 days in coculture, LT-HSCs were found to be in contact with the osteoblastic niche cells at the bottom of the culture plates (Fig. 6, *Aa* and *Ab*). These adherent cells were collected and subsequently isolated into LT-HSCs and osteoblastic niche cells by FACS. As shown in Fig. 6*B*, osteoblastic niche cells derived from nondiabetic mice were still adherent to the bottom in normal glucose medium but lost their adherence in the high-glucose medium (Fig. 6, *Ba* and *Bb*). On the other hand, the osteoblastic niche cells derived from diabetic mice were adherent in the high-glucose medium but in the normal glucose medium (Fig. 6, *Bc*−*Bf*). However, osteoblastic niche cells derived from nondiabetic mice that were cocultured with LT-HSCs derived from diabetic mice adhered to the bottom even in the high-glucose medium (Fig. 6*Bh'*). The survival frequency of LT-HSCs paralleled the existence of osteoblastic niche cells (Fig. 6, *Ba'*−*Bh'*), and LT-HSCs survived in a 7-day coculture system in cases where the osteoblastic niche cells were adherent to the bottoms of the wells (Fig. 6, *Ba'*, *Bd'*, *Bf'*, *Bg'*, and *Bh'*).

Changes in the expression of molecules on LT-HSCs cocultured with osteoblastic niche cells. The expression of molecules on LT-HSCs derived from diabetic or nondiabetic mice was examined after coculture with osteoblastic niche cells derived from diabetic or nondiabetic mice in different glucose conditions. This analysis was only carried out in cases where cells were detected after a 7-day coculture as shown in Fig. 6, *Ba'*, *Bd'*, *Bf'*, *Bg'*, and *Bh'*. We analyzed the N-cadherin, β-catenin, and Tie2 expression on LT-HSCs, as these were shown to be reduced in the in vivo diabetic model mice. N-cadherin expression on diabetic LT-HSCs exposed to diabetic osteoblastic niche cells was significantly reduced compared with that on nondiabetic LH-HSCs exposed to nondiabetic osteoblastic niche cells (Fig. 7, *Aa* and *Ab*). This was also observed for N-cadherin expression on nondiabetic LT-HSCs exposed to diabetic osteoblastic niche cells under high-glucose concentrations compared with those exposed to nondiabetic osteoblastic niche cells (Fig. 7, *Aa* and *Ac*). However, the reduced expression of N-cadherin on diabetic LT-HSCs exposed to diabetic osteoblastic niche cells (Fig. 7*Ab*) was reversed after exposure to nondiabetic osteoblastic niche cells under either normal or high-glucose conditions (Fig. 7, *Ad* and *Ae*). Similarly, the β-catenin expression on LT-HSCs was examined after in vitro coculture with osteoblastic niche cells. The β-catenin expression on diabetic LT-HSCs exposed to diabetic osteoblastic niche cells was significantly reduced compared with that on nondiabetic LH-HSCs exposed to nondiabetic osteoblastic niche cells (Fig. 7, *Ba* and *Bb*). This was reversed after exposure to nondiabetic osteoblastic niche cells

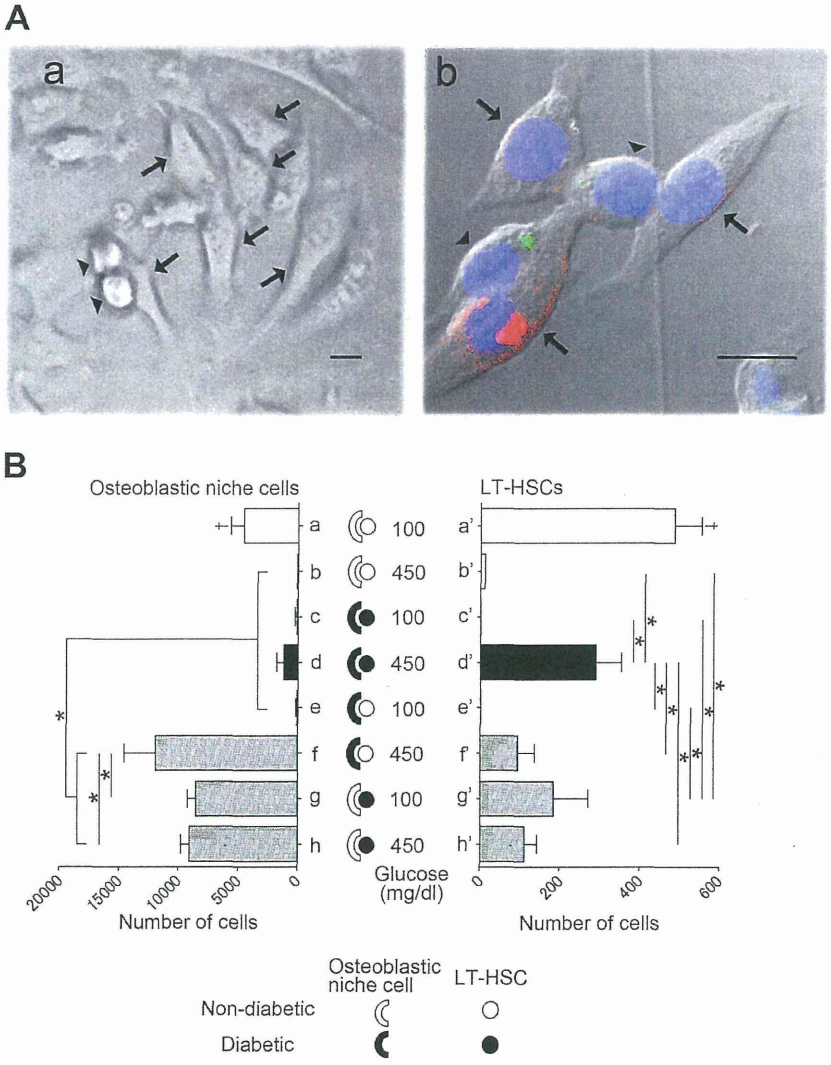

Fig. 6. Findings of the in vitro coculture studies. *Aa*: Phase-contrast microscopy of osteoblastic niche cells (arrows) and LT-HSCs (arrowheads) on *day 7*. Scale bar = 10 μm. *Ab*: Qtracker 525 (green) was detected in the cytoplasm of LT-HSCs (arrow heads) and an OPN-positive reaction (red) was seen in the cytoplasm of osteoblastic niche cells (arrows). Scale bar = 10 μm. *B*: numerical comparison of osteoblastic niche cells and LT-HSCs derived from diabetic and nondiabetic mice cocultured under normal (100 mg/dl) and high glucose (450 mg/dl) conditions. Values are the means ± SD for $n = 6-8$ mice. $^*P < 0.05$ and $\dagger P < 0.05$, compared with other groups.

under normal glucose concentrations (Fig. 7*Bd*). The Tie2 expression on diabetic LT-HSCs exposed to diabetic osteoblastic niche cells was significantly reduced compared with that on nondiabetic LH-HSCs exposed to nondiabetic osteoblastic niche cells (Fig. 7, *Ca* and *Cb*). This was reversed after exposure to nondiabetic osteoblastic niche cells under normal glucose concentrations (Fig. 7*Cd*). The Tie2 expression on nondiabetic LT-HSCs cocultured with diabetic osteoblastic niche cells under high-glucose concentrations was also significantly reduced compared with those exposed to nondiabetic osteoblastic niche cells (Fig. 7, *Ca* and *Cc*).

IBM-BMT for in vivo replacement of osteoblastic niche cells. To confirm the findings obtained from in vitro coculture experiments, we performed IBM-BMTs using OPN^+ and OPN^- cells in different combinations as follows: nondiabetic OPN^+ with nondiabetic OPN^- (Fig. 8*a*), diabetic OPN^+ with diabetic OPN^- (Fig. 8*b*), diabetic OPN^+ with nondiabetic OPN^- (Fig. 8*c*) and nondiabetic OPN^+ with diabetic OPN^- cells (Fig. 8*d*). One week after the bone marrow transplantation, the message level of Tie2 on LT-HSCs was examined. The results showed that the reduced expression of Tie2 on diabetic LT-HSCs exposed to diabetic osteoblastic niche cells (Fig. 8*b*) was completely revered by exposure to nondiabetic osteoblastic niche cells (Fig. 8*d*). On the other hand, the Tie2 expression on nondiabetic LT-HSCs was significantly reduced by exposure to the diabetic osteoblastic niche cells (Fig. 8*c*).

DISCUSSION

Most LT-HSCs are located at the trabecular bone surface of the bone marrow, and their interaction with osteoblastic cells through signaling and cell adhesion molecules appears to be essential to sustain their quiescence and preserve the self-renewal of stem cells during normal hematopoiesis (18). While long-term diabetes is known to impair the mobilization of hematopoietic progenitor cells (7, 22) or diminish the total number of HSCs in both human and mice, few studies have examined the interaction between HSCs and osteoblastic niche cells under diabetic conditions.

In the present study, we isolated LT-HSCs (LSK, $CD34^-$, and $CD135^-$) and osteoblastic niche cells (Lin^- and OPN^+)

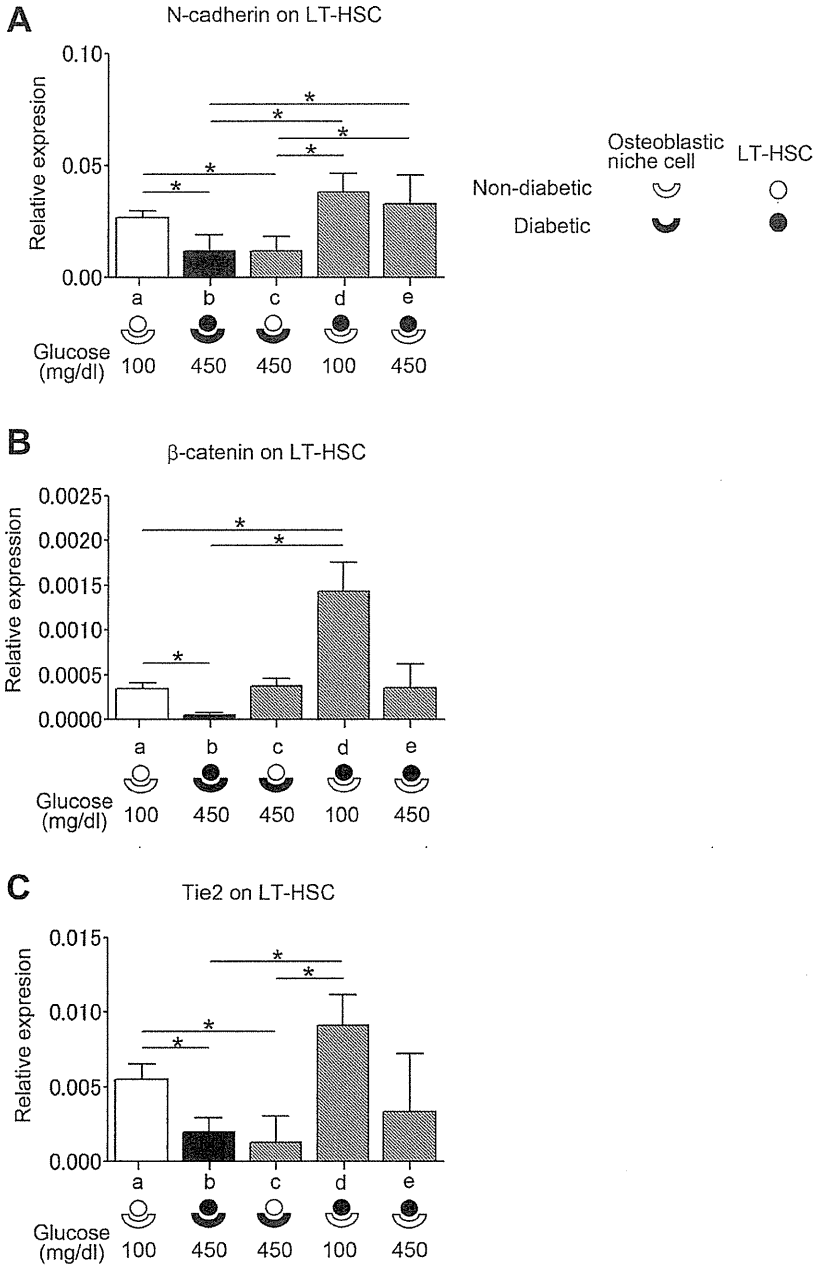

Fig. 7. Expression of molecules on LT-HSCs cocultured with osteoblastic niche cells. mRNA expression levels of N-cadherin (*A*), β-catenin (*B*), and Tie2 (*C*) on nondiabetic (*a* and *c*) or diabetic (*b*, *d*, and *e*) LT-HSCs cocultured with nondiabetic (*a*, *d*, and *e*) or diabetic (*b* and *c*) osteoblastic niche cells cultured under normal (100 mg/dl)- and high (450 mg/dl)-glucose conditions. Values are the means ± SD for $n = 6-8$ mice. $^*P <$ 0.05, compared with other groups.

from the bone marrow of mice with and without diabetes and examined the expression of molecules that regulate the quiescence, apoptosis, and cell adhesion to maintain hematopoietic reconstitution.

FACS analysis showed that the numbers of osteoblastic niche cells and LT-HSCs were reduced, while those of ST-HSCs and MPPs were increased in diabetic mice. Because the numbers of osteoblastic niche cells and LT-HSCs are correlated, the depletion of the former may be caused by depletion of the latter. The observed increase in ST-HSCs and MPPs suggests that, in diabetes, the osteoblastic niche cells fail to maintain the LT-HSCs quiescent, so that their differentiation into ST-HSCs and MPPs was accelerated. Further evidence for this came from the observation that the Ang-1 expression on osteoblastic niche cells and Tie2 expression on HSCs was reduced in diabetic mice. Ang-1 is produced mainly by osteoblastic niche cells, and its receptor tyrosine kinase, Tie2, is expressed on LT-HSCs. Tie2/Ang-1 signaling promotes the tight adhesion of HSCs to osteoblastic niche cells and, under normal conditions, maintains both the quiescence and enhanced survival of HSCs (1).

Although the hematopoiesis activity of LSK cells was not significantly different between the diabetic and nondiabetic mice, as measured by the colony-forming activity in the present study, the bone resorption activity of osteoclasts derived from hematopoietic progenitors (3) was abnormally increased

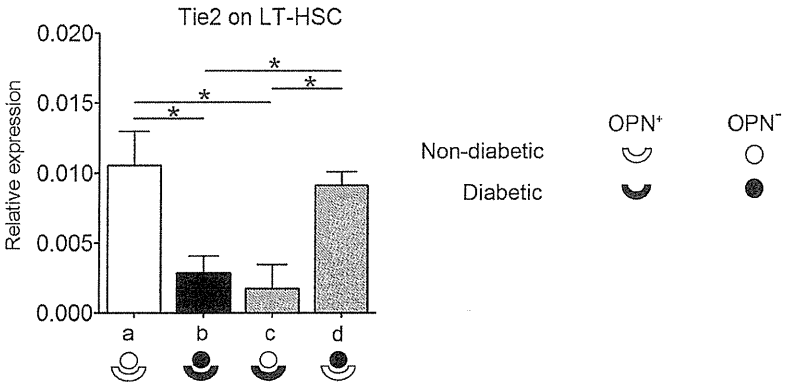

Fig. 8. Expression of Tie2 on LT-HSCs in intrabone marrow-bone marrow transplantation (IBM-BMT) mice. Mixture of nondiabetic (*a* and *c*) or diabetic (*b* and *d*) OPN$^+$ cells and nondiabetic (*a* and *d*) or diabetic (*b* and *c*) OPN$^-$ cells were transplanted into the left tibia of mice. mRNA expression of Tie2 on LT-HSCs at 7 days after IBM-BMT. The values are means ± SD for $n = 4-5$ mice. *$P < 0.05$, compared with other groups.

in the diabetic mice. Hyperactivity of osteoclasts in the diabetic state has been shown in a previous study (24).

The present results also revealed that the expression of N-cadherin on LT-HSCs and the expression of β_1-integrin on osteoblastic niche cells were reduced in diabetic mice. As N-cadherin-mediated adhesion mediates the slow cycling and quiescence of HSCs (1, 11, 12), and β_1-integrin is essential for the interaction between bone marrow niche cells and HSCs and for regulating the initial self-renewing HSC division and survival (10), our findings suggest that HSCs failed to maintain quiescence, self-renewal, and survival under diabetic conditions.

The Wnt signaling cascade is triggered upon binding to a coreceptor complex, including Fzd and LRP5/6 (2, 8, 15, 29). Wnt, Fzd, and Dkk are included in the β-catenin phosphorylation complex, which leads to β-catenin degradation, and Dkk binds to and inactivates the signaling from LRP5/6 receptors. Wnt/β-catenin signaling may play a crucial role in the maintenance of the self-renewal activity in bone marrow. In the present study, we showed that both the LRP6 expression on LT-HSCs and the β-catenin expression on LH-HSCs were reduced in diabetic mice, suggesting that diabetes impairs the Wnt/β-catenin pathway, resulting in abnormalities in the reconstituting of HSCs.

Chemokines and their receptors control the behavior of HSCs by regulating the migration, homing, and release of HSCs within the bone marrow. The importance of CXCL12/CXCR4 signaling was previously demonstrated in CXCL12$^{-/-}$ and CXCR4$^{-/-}$ mice (33, 37), which have a severe defect in their bone marrow myeloid progenitors. We herein demonstrated that diabetes induced the depletion of CXCL12 expression by osteoblastic niche cells, suggesting that there is an impaired interaction between osteoblastic niche cells and LT-HSCs in the bone marrow in diabetic mice.

Our in vitro coculture of LT-HSCs and osteoblastic niche cells in normal and high-glucose media aimed to mimic the diabetic and nondiabetic microenvironments in the bone marrow niche. The morphological features of the interactions between osteoblastic niche cells and LT-HSCs in the coculture experiments were shown to be similar to the in vivo localization of osteoblastic niche cells and LT-HSCs in the bone marrow sections. Furthermore, the staining pattern was the same between nondiabetic and diabetic mice, suggesting that the surface phenotype of osteoblastic niche cells and LT-HSCs may remain in diabetic mice, separate from their functional abnormalities. In coculture experiments, osteoblastic niche cells derived from nondiabetic mice were found to adhere to the culture plate for 7 days under normoglycemic, but not hyperglycemic, conditions. The reverse was true for osteoblastic niche cells derived from diabetic mice, suggesting that such cells adapt to higher glucose concentrations. The survival frequency of LT-HSCs paralleled the existence of osteoblastic niche cells. Therefore, our coculture experiments provide an adequate microenvironment for keeping LT-HSCs in contact with osteoblastic niche cells and for maintaining the stemness for at least 7 days. Attempts have previously been made to reconstitute a bone marrow niche using three-dimensional (17, 28) or low oxygen tension (13) coculture systems. However, as shown here, a conventional two-dimensional coculture appears to be sufficient.

The coculture experiments showed the same abnormalities in the LT-HSC expression of N-cadherin, β-catenin, and Tie2 seen in vivo in the diabetic mice. The use of different coculture combinations of LT-HSCs and osteoblastic niche cells led to several important findings: nondiabetic LT-HSCs with diabetic osteoblastic niche cells led to reduced expression of these molecules, perhaps through impairment of the self-renewal, survival, and quiescence of HSCs. Most interestingly, the in vitro exposure of diabetic LT-HSCs to nondiabetic osteoblastic niche cells successfully reversed these abnormalities in expression. Although it is known that diabetes induces impaired hematopoietic stem/progenitor cell mobilization and repopulation by altering the functions of the bone marrow niche (7, 27), no previous studies have shown the effects of the replacement of bone marrow niche cells on their partner HSCs. Our in vivo IBM-BMT experiments revealed that the replacement of osteoblastic niche cells could successfully reverse the abnormalities in LT-HSCs caused by diabetes.

In summary, we have demonstrated that diabetes induces impairments in the expression of molecules on both LT-HSCs and osteoblastic niche cells, which are essential for maintaining the quiescence and reconstitution of HSCs in the bone marrow niche. Normal LT-HSCs displayed abnormal expression of these molecules when exposed to diabetic osteoblastic niche cells, but this abnormality could be reversed after exposure to nondiabetic osteoblastic niche cells. Although it is not known at present how diabetic metabolism impairs the osteoblastic niche cells, the present results provide important information for the treatment of diabetes-induced HSC abnormalities, which could include the replacement of bone marrow niche cells.

ACKNOWLEDGMENTS

We thank Susumu Ikehara and Ming Li for support for IBM-BMT.

GRANTS

This work was supported by Grant-in-Aid for Scientific Research 23592223 (to K. Iba) and 21390054 (to M. Fujimiya) from the Ministry of Education, Culture, Sports, Science, and Technology, Japan.

DISCLOSURES

No conflicts of interest, financial or otherwise, are declared by the author(s).

AUTHOR CONTRIBUTIONS

Author contributions: H.C. and K.A. performed experiments; H.C., K.A., K.I., and K.N. analyzed data; H.C., K.A., K.I., K.N., and T.Y. interpreted results of experiments; H.C. and K.A. prepared figures; H.C., K.A., and M.F. drafted manuscript; K.A. and M.F. approved final version of manuscript; K.I., T.Y., and M.F. conception and design of research.

REFERENCES

1. **Arai F, Suda T.** Maintenance of quiescent hematopoietic stem cells in the osteoblastic niche. *Ann NY Acad Sci* 106: 41–53, 2007.
2. **Baron R, Rawadi G.** Targeting the Wnt/beta-catenin pathway to regulate bone formation in the adult skeleton. *Endocrinology* 148: 2635–2643, 2007.
3. **Bar-Shavit Z.** The osteoclast: a multinucleated, hematopoietic-origin, bone-resorbing osteoimmune cell. *J Cell Biochem* 102: 1130–1139, 2007.
4. **Chan L, Terashima T, Fujimiya M, Kojima H.** Chronic diabetic complications: the body's adaptive response to hyperglycemia gone awry? *Trans Am Clin Climatol Assoc* 117: 341–351, 2006.
5. **Ehninger A, Trumpp A.** The bone marrow stem cell niche grows up: mesenchymal stem cells and macrophages move in. *J Exp Med* 208: 421–428, 2011.
6. **Fadini GP, Boscaro E, de Kreutzenberg S, Agostini C, Seeger F, Dimmeler S, Zeiher A, Tiengo A, Avogaro A.** Time course and mechanisms of circulating progenitor cell reduction in the natural history of type 2 diabetes. *Diabetes Care* 33: 1097–1102, 2010.
7. **Ferraro F, Lymperi S, Méndez-Ferrer S, Saez B, Spencer JA, Yeap BY, Masselli E, Graiani G, Prezioso L, Rizzini EL, Mangoni M, Rizzoli V, Sykes SM, Lin CP, Frenette PS, Quaini F, Scadden DT.** Diabetes impairs hematopoietic stem cell mobilization by altering niche function. *Sci Transl Med* 3: 101–104, 2011.
8. **Fleming HE, Janzen V, Lo Celso C, Guo J, Leahy KM, Kronenberg HM, Scadden DT.** Wnt signaling in the niche enforces hematopoietic stem cell quiescence and is necessary to preserve self-renewal in vivo. *Cell Stem Cell* 2: 274–283, 2008.
9. **Fujimiya M, Kojima H, Ichinose M, Arai R, Kimura H, Kashiwagi A, Chan L.** Fusion of proinsulin-producing bone marrow-derived cells with hepatocytes in diabetes. *Proc Natl Acad Sci USA* 104: 4030–4035, 2007.
10. **Gottschling S, Saffrich R, Seckinger A, Krause U, Horsch K, Miesala K, Ho AD.** Human mesenchymal stromal cells regulate initial self-renewing divisions of hematopoietic progenitor cells by a beta1-integrin-dependent mechanism. *Stem Cells* 25: 798–806, 2007.
11. **Haug JS, He XC, Grindley JC, Wunderlich JP, Gaudenz K, Ross JT, Paulson A, Wagner KP, Xie Y, Zhu R, Yin T, Perry JM, Hembree MJ, Redenbaugh EP, Radice GL, Seidel C, Li L.** N-cadherin expression level distinguished reserved versus primed states of hematopoietic stem cells. *Cell Stem Cells* 2: 367–379, 2008.
12. **Hosokawa K, Arai F, Yoshihara H, Iwasaki H, Nakamura Y, Gomei Y, Suda T.** Knockdown of N-cadherin suppresses the long-term engraftment of hematopoietic stem cells. *Blood* 116: 554–563, 2010.
13. **Jing D, Wobus M, Poitz DM, Bornhauser M, Ehninger G, Ordemann R.** Oxygen tension plays a critical role in the hematopoieticmicroenvironment in vitro. *Hematologica* 97: 331–339, 2012.
14. **Kawamoto T.** Use of a new adhesive film for the preparation of multi-purpose fresh-frozen sections from hard tissues, whole-animals, insects and plants. *Arch Histol Cytol* 66: 123–143, 2003.
15. **Kirstetter P, Anderson K, Porse BT, Jacobsen SE, Nerlov C.** Activation of the canonical Wnt pathway leads to loss of hematopoietic stem cell repopulation and multilineage differentiation block. *Nat Immunol* 7: 1048–1056, 2006.
16. **Kushida T, Inaba M, Hisha H, Ichioka N, Esumi T, Ogawa R, Iida H, Ikehara S.** Intra-bone marrow injection of allogeneic bone marrow cells: a powerful new strategy for treatment of intractable autoimmune diseases in MRL/lpr mice. *Blood* 97: 3292–3299, 2001.
17. **Leisten I, Kramann R, Ventura Ferreira MS, Bovi M, Neuss S, Ziegler P, Wagner W, Knüchel R, Schneider RK.** 3D coculture of hematopoietic stem and progenitor cells and mesenchymal stem cells in collagen scaffolds as a model of the hematopoietic niche. *Biomaterials* 3: 1736–1747, 2012.
18. **Li L, Bhatia R.** Stem cell quiescence. *Clin Cancer Res* 17: 4936–4941, 2011.
19. **Loomans CJ, de Koning EJ, Staal FJ, Rookmaaker MB, Verseyden C, de Boer HC, Verhaar MC, Braam B, Rabelink TJ, van Zonneveld AJ.** Endothelial progenitor cell dysfunction: a novel concept in the pathogenesis of vascular complications of type 1 diabetes. *Diabetes* 53: 195–199, 2004.
20. **Ma Z, Wirström T, Borg LA, Larsson-Nyrén G, Hals I, Bondo-Hansen J, Grill V, Björklund A.** Diabetes reduces β-cell mitochondria and induces distinct morphological abnormalities, which are reproducible by high glucose in vitro with attendant dysfunction. *Islets* 4: 233–242, 2012.
21. **Mayack SR, Shadrach JL, Kim FS, Wagers AJ.** Systemic signals regulate ageing and rejuvenation of blood stem cell niches. *Nature* 463: 495–500, 2010.
22. **Méndez-Ferrer S, Michurina TV, Ferraro F, Mazloom AR, Macarthur BD, Lira SA, Scadden DT, Ma'ayan A, Enikolopov GN, Frenette PS.** Mesenchymal and haematopoietic stem cells form a unique bone marrow niche. *Nature* 466: 829–834, 2010.
23. **Mercier FE, Ragu C, Scadden DT.** The bone marrow at the crossroads of blood and immunity. *Nat Rev Immunol* 12: 49–60, 2012.
24. **Motyl K, McCabe LR.** Streptozotocin, type I diabetes severity and bone. *Biol Proced Online* 11: 296–315, 2009.
25. **Ogawa M.** Differentiation and proliferation of hematopoietic stem cells. *Blood* 81: 2844–2853, 1993.
26. **Omatsu Y, Sugiyama T, Kohara H, Kondoh G, Fujii N, Kohno K, Nagasawa T.** The essential functions of adipo-osteogenic progenitors as the hematopoietic stem and progenitor cell niche. *Immunity* 33: 387–399, 2010.
27. **Orlandi A, Chavakis E, Seeger F, Tjwa M, Zeiher AM, Dimmeler S.** Long-term diabetes impairs repopulation of hematopoietic progenitor cells and dysregulates the cytokine expression in the bone marrow microenvironment in mice. *Basic Res Cardiol* 105: 703–712, 2010.
28. **Sharma MB, Limaye LS, Kale VP.** Mimicking the functional hematopoietic stem cell niche in vitro: recapitulation of marrow physiology by hydrogel-based three-dimensional cultures of mesenchymal stromal cells. *Hematologica* 97: 651–660, 2012.
29. **Suda T, Arai F.** Wnt signaling in the niche. *Cell* 132: 729–730, 2008.
30. **Tepper OM, Carr J, Allen RJ Jr, Chang CC, Lin Tanaka R CD, Gupta SM, Levine JP, Saadeh PB, Warren SM.** Decreased circulating progenitor cell number and failed mechanisms of stromal cell-derived factor-1alpha mediated bone marrow mobilization impair diabetic tissue repair. *Diabetes* 59: 1974–1983, 2010.
31. **Terashima T, Kojima H, Fujimiya M, Matsumura K, Oi J, Hara M, Kashiwagi A, Kimura H, Yasuda H, Chan L.** The fusion of bone-marrow-derived proinsulin-expressing cells with nerve cells underlies diabetic neuropathy. *Proc Natl Acad Sci USA* 102: 12525–12530, 2005.
32. **Tariq M, Masoud MS, Mehmood A, Khan SN, Riazuddin S.** Stromal cell derived factor-1alpha protects stem cell derived insulin-producing cells from glucotoxicity under high glucose conditions in-vitro and ameliorates drug induced diabetes in rats. *J Transl Med* 11: 115, 2013.
33. **Tzeng YS, Li H, Kang YL, Chen WC, Cheng WC, Lai DM.** Loss of Cxcl12/Sdf-1 in adult mice decreases the quiescent state of hematopoietic stem/progenitor cells and alters the pattern of hematopoietic regeneration after myelosuppression. *Blood* 117: 429–439, 2011.
34. **Wang DL, Wagers AJ.** Dynamic niches in the origination and differentiation of haematopoietic stem cells. *Nat Rev Mol Cell Biol* 12: 643–655, 2011.
35. **Weksberg DC, Chambers SM, Boles NC, Goodell MA.** CD150- side population cells represent a functionally distinct population of long-term hematopoietic stem cells. *Blood* 111: 2444–2451, 2008.
36. **Yamashita T, Fujimiya M, Nagaishi K, Ataka K, Tanaka M, Yoshida H, Tsuchihashi K, Shimamoto K, Miura T.** Fusion of bone marrow-derived cells with renal tubules contributes to renal dysfunction in diabetic nephropathy. *FASEB J* 26: 1559–1568, 2012.
37. **Zou YR, Kottmann AH, Kuroda M, Taniuchi I, Littman DR.** Function of the chemokine receptor CXCR4 in haematopoiesis and in cerebellar development. *Nature* 393: 595–599, 1998.

HEPATOLOGY
Official Journal of the American Association for the Study of Liver Diseases

Mesenchymal Stem Cell Therapy Ameliorates Diabetic Hepatocyte Damage in Mice by Inhibiting Infiltration of Bone Marrow–Derived Cells

Kanna Nagaishi,[1] Koji Ataka,[1] Eijiro Echizen,[1] Yoshiaki Arimura,[2] and Mineko Fujimiya[1]

Although mesenchymal stem cells (MSCs) have been implicated in hepatic injury, the mechanism through which they contribute to diabetic liver disease has not been clarified. In this study, we investigated the effects of MSC therapy on diabetic liver damage with a focus on the role of bone-marrow–derived cells (BMDCs), which infiltrate the liver, and elucidated the mechanism mediating this process. Rat bone-marrow (BM)-derived MSCs were administered to high-fat diet (HFD)-induced type 2 diabetic mice and streptozotocin (STZ)-induced insulin-deficient diabetic mice. MSC-conditioned medium (MSC-CM) was also administered to examine the trophic effects of MSCs on liver damage. Therapeutic effects of MSCs were analyzed by assessing serum liver enzyme levels and histological findings. Kinetic and molecular profiles of BMDCs in the liver were evaluated using BM-chimeric mice. Curative effects of MSC and MSC-CM therapies were similar because both ameliorated the aggravation of aspartate aminotransferase and alanine aminotransferase at 8 weeks of treatment, despite persistent hyperlipidemia and hyperinsulinemia in HFD-diabetic mice and persistent hyperglycemia in STZ-diabetic mice. Furthermore, both therapies suppressed the abnormal infiltration of BMDCs into the liver, reversed excessive expression of proinflammatory cytokines in parenchymal cells, and regulated proliferation and survival signaling in the liver in both HFD- and STZ-diabetic mice. In addition to inducing hepatocyte regeneration in STZ-diabetic mice, both therapies also prevented excessive lipid accumulation and apoptosis of hepatocytes and reversed insulin resistance (IR) in HFD-diabetic mice. *Conclusion:* MSC therapy is a powerful tool for repairing diabetic hepatocyte damage by inhibiting inflammatory reactions induced by BMDCs and IR. These effects are likely the result of humoral factors derived from MSCs. (HEPATOLOGY 2014;59:1816-1829)

The incidence of diabetes is second only to that of cancer. Type 2 diabetes (T2D) is associated with nonalcoholic fatty liver disease (NAFLD), which progresses to nonalcoholic steatohepatitis (NASH). Insulin resistance (IR), fatty acid accumulation in the liver, and proinflammatory cytokine expression are the main factors that increase susceptibility to hepatocyte damage in NASH.[1] In addition, the preva-

Abbreviations: Akt, protein kinase B; ALT, alanine aminotransferase; ANOVA, analysis of variance; AST, aspartate aminotransferase; Bcl2, B-cell lymphoma 2; BM, bone marrow; BMDC, BM-derived cell; BMT, BM transplantation; b.w., body weight; Ccr2, C-C chemokine receptor 2; C/EBPα, CCAAT/enhancer-binding protein alpha; ERK, extracellular signal-regulated kinase; FABP4, fatty-acid–binding protein 4; FACS, fluorescence-activated cell sorting; Fizz1, found in inflammatory zone 1; FoxO1, forkhead box O1; GFP, green fluorescence protein; GLUT2, glucose transporter 2; HFD, high-fat diet; HNF-4, hepatocyte nuclear factor 4; HOMA-IR, homeostasis model assessment-estimated IR; HSECs, hepatic sinusoidal endothelial cells; ICAM-1, intracellular adhesion molecule 1; IL, interleukin; IP, intraperitoneal; IR, insulin resistance; Irs-2, insulin receptor substrate 2; JNK, c-Jun amino-terminal kinase; MAPK, mitogen-activated protein kinase; MCs, mononuclear cells; MCP, monocyte chemotactic protein; Mrc1, mannose receptor C type 1; MSC, mesenchymal stem cell; MSC-CM, MSC-conditioned medium; NAFLD, nonalcoholic fatty liver disease; NASH, nonalcoholic steatohepatitis; NF-κB, nuclear factor kappa light-chain enhancer of activated B cells; PBMCs, peripheral blood mononuclear cells; PBS, phosphate-buffered saline; RBCs, red blood cells; SE, standard error; SECs, sinusoidal endothelial cells; SREBP-1c, sterol response element-binding protein 1c; STZ, streptozotocin; T2D, type 2 diabetes; TGF-β1, transforming growth factor beta 1; Tg, transgenic; TLR4, Toll-like receptor 4; TNFα, tumor necrosis factor alpha; Trop2, trophoblast cell-surface antigen 2; TUNEL, terminal deoxynucleotidyl transferase-mediated dUTP nick-end labeling.

From the [1]Second Department of Anatomy and [2]First Department of Internal Medicine, Sapporo Medical University, School of Medicine, Sapporo, Japan.

Received January 13, 2013; accepted December 12, 2013.

This work was supported, in part, by a Grant-in-Aid for Scientific Research (C) in Japan (to K.N.).

lence of elevated alanine aminotransferase (ALT) is also 3- to 4-fold higher in patients with type 1 diabetes, compared with the general population, with a marked accumulation of glycogen and steatohepatitis.[2] Therefore, the therapeutic approach for reversing hepatocyte damage as well as IR caused by diabetes is a matter of significance.

Previously, we detected proinsulin- and tumor necrosis factor alpha (TNFα)-producing abnormal cells in the bone marrow (BM) of high-fat diet (HFD)-induced and streptozotocin (STZ)-induced diabetic mice and showed that these cells migrated from the BM to infiltrate the liver.[3] In diabetes, BM-derived cells (BMDCs) infiltrate the liver excessively and subsequently produce cytotoxic chemokines or fuse with hepatocytes, causing parenchymal cells to produce proinsulin and cytotoxic TNFα, which leads to the degeneration or apoptosis of target cells.[4,5] These findings, in the context of diabetes, suggest that hyperglycemia is the primary cause of abnormal cells in BM and that infiltration of abnormal BMDCs in the liver may be the secondary cause of hepatocyte degeneration.

Intravenous transplantation of BM-derived mesenchymal stem cells (MSCs) has been demonstrated to be effective for diabetes. However, most previous studies have investigated the potential role of BM-derived MSCs in regenerating β cells and for subsequently improving hyperglycemia in type 1 or insulin deficiency diabetes models.[6,7] A limited number of reports have shown the effects of BM-derived MSCs on T2D with hepatocyte damage and IR.[8,9] Previous studies have reported that MSC therapy reversed hepatic enzyme levels in HFD-induced diabetic mice and suppressed proinflammatory cytokine expression in the liver, but MSC therapy failed to reverse obesity, hypercholesterolemia, hyperglycemia, and IR.[8] Another study showed an improvement in IR in an HFD-induced diabetes model[9]; however, rats received an STZ injection in addition to a 2-week HFD and the model was also an insulin deficiency model, rather than a hyperinsulinemia T2D model, so the therapeutic effects of MSCs were derived from pancreatic β-cell regeneration. To date, no reports have shown the effects of MSCs on IR associated with NAFLD or NASH in T2D with persistent hyperglycemia and -insulinemia.

BM-derived MSCs are known to exert immunoregulatory and antiapoptotic effects.[10] The mechanism of action underlying MSC therapy is suggested to mediate the cell complement effect by cell differentiation or various paracrine effects through trophic factors secreted by MSCs.[11] In fact, because systemic infusion of MSC-conditioned medium (MSC-CM) has been shown to ameliorate hepatocellular death and stimulate hepatocyte regeneration in a rat model of fulminant hepatic failure,[12] the mechanism of action of systemically injected MSCs might be the result of their released humoral factors. This hypothesis is conceivable because the number of MSCs logged after systemic injection is remarkably small, considering their powerful therapeutic effects.

In this study, we aimed to investigate the following effects resulting from intravenous administration of MSCs, which contributed to a common, distinctive pathogenesis in liver of mice in an HFD-induced T2D model and an STZ-injected insulin deficiency model: (1) suppression of abnormal BMDC infiltration into the liver; (2) amelioration of hepatocyte degeneration induced by proinflammatory cytokine expression and subsequent apoptosis; (3) enhancement of hepatocyte regeneration; and (4) reduction of IR associated with lipid accumulation and proinflammatory cytokine expression in the liver. To clarify the therapeutic effects of MSC-derived trophic factors, effects of MSC infusion were compared in parallel with those of MSC-CM administration. The present findings may provide new perspectives on therapeutic approaches to diabetes-induced hepatic damage.

Materials and Methods

Animals and BM Transplantation. C57BL/6J mice and C57BL/6-Tg (CAG-EGFP; green fluorescence protein-transgenic [GFP-Tg]) mice were purchased from Japan SLC (Shizuoka, Japan). GFP-BM chimeric mice were produced by lethal irradiation

Address reprint requests to: Mineko Fujimiya, M.D., Ph.D., Second Department of Anatomy, Sapporo Medical University School of Medicine, S-1, W-17, Chuo-ku, Sapporo 060-8556, Japan. E-mail: fujimiya@sapmed.ac.jp; fax: +81-11-618-4288.

View this article online at wileyonlinelibrary.com.
DOI 10.1002/hep.26975
Potential conflict of interest: Nothing to report.
Additional Supporting Information may be found in the online version of this article.

(9 Gy) and systemic injection with 4-6 × 10^6 BM cells isolated from GFP-Tg mice. Four weeks after BM transplantation (BMT), hyperglycemia was induced by feeding a HFD containing 60% lard (High-Fat Diet 32; Clea Japan Inc., Tokyo, Japan) or by a single intraperitoneal (IP) injection of STZ (150 mg/kg; Wako, Osaka, Japan) dissolved in citrate buffer (pH 4.5). Controls were fed a normal diet or treated with an IP injection of buffer. After 28 weeks of HFD feeding, mice were administered 1 × 10^4 MSCs/g body weight (b.w.) four times every 2 weeks (HFD-MSC), whereas controls received vehicle (HFD-vehicle; Fig. 1A). At 4 weeks after STZ injection, mice were administered twice with 1 × 10^4 MSCs/g b.w. every 4 weeks (STZ-MSC), whereas controls received vehicle (STZ-vehicle; Fig. 2A). This study was performed with the approval of the animal experiment committee of Sapporo Medical University (Sapporo, Japan).

Isolation, Culture, and Characterization of Rat BM-Derived MSCs. Rat MSCs were harvested from BM of 8-week-old Lewis rats (Charles River Laboratories Japan Inc., Yokohama, Japan) and cultured as described previously.[13] Immunophenotype and differentiation potential of rat MSCs were then determined (Supporting Fig. 1A,B).

Preparation of MSC-CM From Rat MSCs. Rat MSCs (2 × 10^5 cells) were seeded in 150-cm^2 culture dishes. When MSCs reached confluence, the medium was changed to serum-free medium and cultured for 24 hours. Then, the supernatant was collected and further concentrated (final concentration: 1 mg/mL) as MSC-CM by ultrafiltration using centrifugal filter units with a 10-kDa cutoff (Ultracel-10K; Millipore, Billerica, MA), following the manufacturer's instructions.

Intravenous Administration of MSCs and MSC-CM. MSCs (1 × 10^4 MSCs/g b.w. per animal suspended in 200 μL of phosphate-buffered saline [PBS]) or MSC-CM (2 mg/kg/day) were administered through the tail vein of mice after induction of diabetes (Fig. 1D). Vehicle administration was PBS for MSC therapy. We also administered MSC-CM to diabetic mice daily for 8 weeks (Fig. 2D). Vehicle administration was serum-free medium that was concentrated using the same procedure as that for the conditioned medium used for MSC-CM therapy.

Detection of Donor MSCs. HFD- and STZ-induced diabetic mice without BMT were administered MSCs labeled with PKH26 Red Fluorescent Cell Linker Kits (Sigma-Aldrich, Saint Louis, MO), sacrificed at 1, 2, or 4 weeks after MSC injection, and lung, liver, kidney, spleen, and bone were obtained. Organs were immersed in 4% paraformaldehyde, and bone was decalcified with 0.5 M of ethylenediaminetetraacetic acid (Wako, Osaka, Japan) for 2 days. Frozen sections of each organ were stained with 4',6-diamidino-2-phenylindole (Dojindo Laboratories, *Kumamoto*, Japan) at 0.1 mg/mL. Distribution of MSCs expressing red fluorescence in each organ was observed by confocal laser scanning microscopy (LSM 510; Carl Zeiss, Oberkochen, German). The ratio of MSCs distributed in each organ was determined by counting PKH26-positive cells in 20 randomly selected visual fields at 100× magnification per mouse (n = 3-5) and compensated by the number of MSCs given to each mouse.

Quantitative Analysis of the GFP-Positive Area. The mean percentage of the area occupied by GFP-positive cells in the liver of each animal was determined by sampling 20 randomly selected visual fields at 100× magnification using the NIS element BR 3.0 image analyzing system.

Isolation of GFP-Positive BMDCs From the Liver by Fluorescence-Activated Cell Sorting. GFP-positive BMDCs were isolated from the liver. Pieces of liver were removed, minced, and treated with 400 U/mL of collagenase (Wako) diluted in PBS for 30 minutes at 37°C. Dissolved tissue was further minced and filtered with a 100-μm pore cell strainer and centrifuged for 5 minutes at 300×*g*. The cell pellet was treated with red blood cell (RBC) lysis buffer (Qiagen, Venlo, the Netherlands) to remove remaining RBCs and washed with 2% fetal bovine serum in 0.1 M of PBS. GFP-positive BMDCs were isolated by fluorescence-activated cell sorting (FACS; Aria; BD Biosciences, Tokyo, Japan).

Isolation of Mononuclear Cells From Peripheral Blood. Peripheral blood mononuclear cells (PBMCs) were isolated by the Ficoll-Paque (GE Healthcare Japan, Tokyo, Japan) density-gradient separation method, following the manufacturer's instructions.

Statistical Analysis. Data are expressed as mean ± standard error (SE) values. Analysis of variance (ANOVA) was employed for multiple comparisons. Two-way repeated-measures (mixed between-within subjects) ANOVA, followed by Bonferroni's test, was used for serial assessment. Differences were considered significant at $P < 0.05$ in all two-tailed tests.

Results

Differentiation of Rat BM-Derived MSCs Into Multiple Mesenchymal Lineages. Specific surface antigens for rat MSCs were detected by FACS. CD90 was positively detected, whereas CD11b, CD31, CD43,

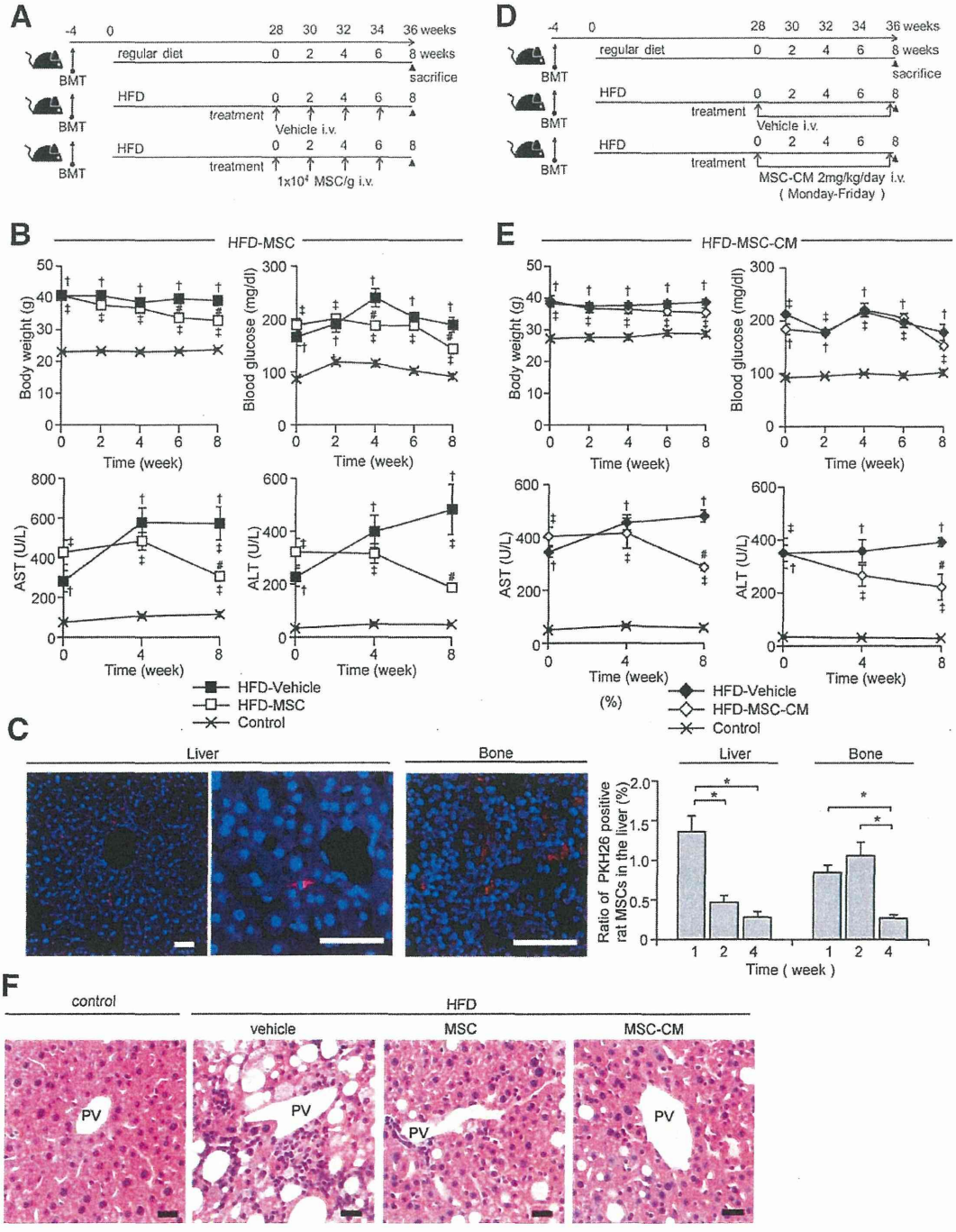

Fig. 1. Rat MSC therapy for HFD-induced diabetic mice. Protocol for MSC (A) and MSC-CM (D) therapies in HFD-diabetic mice. (B and E) Changes in body-weight and serum blood-glucose levels, AST, and ALT after beginning rMSC therapy. Data are expressed as mean ± SE values of 5-10 animals. †$P < 0.05$, HFD-vehicle versus control; ‡$P < 0.05$, HFD-MSC or HFD-MSC-CM versus control; #$P < 0.05$, HFD-MSC or HFD-MSC-CM versus HFD-vehicle. (C) Distribution of rMSCs marked with PKH26 in liver and femur of HFD mice at 1 week after initial rMSC injection are shown in left panel. Changes in the ratio of PKH26-positive cells in liver and bone at 1, 2, and 4 weeks after initial rMSC injection are shown in right panel. Bar, 50 μm. (F) Histological findings of the periportal area in the hematoxylin and eosin-stained liver section 8 weeks after initial MSC therapy. Bar, 20 μm.

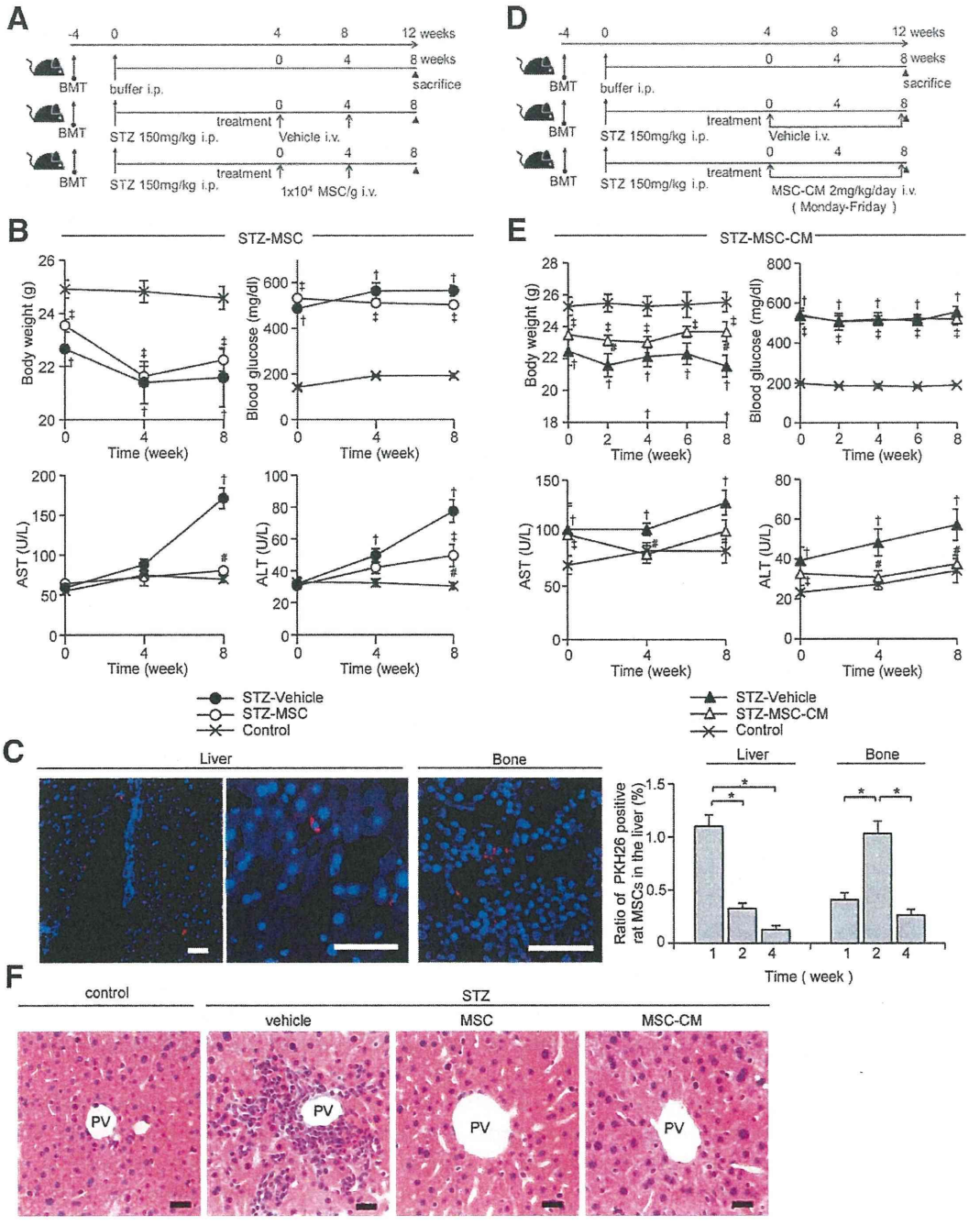

Fig. 2. Rat MSC therapy for STZ-induced diabetic mice. Protocol for MSC (A) and MSC-CM (D) therapies in STZ-diabetic mice. (B and E) Changes in body-weight and serum blood-glucose levels, AST, and ALT after beginning rMSC therapy. Data are expressed as mean ± SE values of 5-10 animals. †$P < 0.05$, STZ-vehicle versus control; ‡$P < 0.05$, STZ-MSC or STZ-MSC-CM versus control; #$P < 0.05$, STZ-MSC or STZ-MSC-CM versus STZ-vehicle. (C) Distribution of rMSCs marked with PKH26 in liver and femur of STZ mice at 1 week after initial rMSC injection were shown in the left panel. Changes in the ratio of PKH26-positive cells in liver and bone at 1, 2, and 4 weeks after initial rMSC injection are shown in right panel. Bar, 50 μm. (F) Histological findings of the periportal area in the hematoxylin and eosin-stained liver section 8 weeks after the initial MSC therapy. Bar, 20 μm.

CD44, and CD45 were negative (Supporting Fig. 1A). MSCs exhibited osteogenic, adipose, and chondrogenic differentiation ability (Supporting Fig. 1B).

MSC Therapy Prevented Liver Damage in HFD- and STZ-Diabetic Mice. MSC treatment successfully reversed hepatocyte damage caused by diabetes, as

indicated by recovery of aspartate aminotransferase (AST) and ALT levels after 8 weeks of treatment in both HFD-MSC (Fig. 1B) and STZ-MSC mice (Fig. 2B), compared to HFD- and STZ-vehicle mice, respectively. Body-weight and blood-glucose levels were mildly ameliorated in HFD-MSC mice, compared to HFD-vehicle mice (Fig. 1B); however, they were unchanged between STZ-vehicle and STZ-MSC (Fig. 2B).

Administered MSCs Detected in Liver and BM of HFD- and STZ-Diabetic Mice. PKH26-positive MSCs were detected in the periportal area and in the parenchyma of the liver, as well as around the marrow sinusoid and in the bone parenchyma in HFD-MSC and STZ-MSC mice (Figs. 1C and 2C). Detection frequency of administered MSCs was changed, depending on the time. The number of MSCs distributed in the liver decreased over time, whereas it was increased for 2 weeks after administration before decreasing thereafter in bone. However, the number of PKH26-positive MSCs detected was too small to account for the direct effect of MSCs, such as cell-cell contact or cell differentiation.

MSC-CM Therapy Prevented Liver Damage in HFD- and STZ-Diabetic Mice, Similar to MSCs. Similar to the effect of cell therapy, MSC-CM injections successfully reversed hepatocyte damage, as indicated by recovery of AST and ALT levels after 8 weeks of initial administration in HFD-diabetic mice and after 4 weeks of initial administration in STZ-diabetic mice (Figs. 1E and 2E). In contrast to cell therapy, there were no differences in body-weight or fasting blood-glucose levels between HFD-MSC-CM and HFD-vehicle mice (Fig. 1E). Body weight recovered in STZ-MSC-CM mice, whereas glucose level remained unchanged (Fig. 2E). The MSC-CM dose of 2 mg/kg/day was considered suitable because our preliminary study showed that 1 mg/kg/day was not effective, whereas 4 mg/kg/day proved toxic and caused loss of body weight (data not shown). Injection of MSC-CM caused no fever in mice.

MSC and MSC-CM Therapies Prevented Histopathological Damage in Liver of HFD- and STZ-Diabetic Mice. Significant infiltration of inflammatory cells into the periportal area and numerous deposition of lipid droplets, which had a round vacuolar appearance, in hepatocytes were detected in HFD-vehicle mice (Fig. 1F). These pathological findings were attenuated in HFD-MSC and HFD-MSC-CM mice. Whereas massive accumulation of inflammatory cells in the periportal area and destruction of the round ligament of the liver were observed in STZ-vehicle mice (Fig. 2F), MSC and MSC-CM therapy suppressed excessive infiltration of inflammatory cells and reversed the structure of hepatic tissue.

MSC and MSC-CM Therapies Suppressed Excessive Infiltration of BMDCs, Especially Macrophages, in Liver of HFD- and STZ-Diabetic Mice. Areas occupied by BMDCs (green) were significantly larger in HFD- and STZ-vehicle mice, compared to controls (Figs. 3A and 4A, left). BMDCs massively infiltrated not only the hepatic sinusoid, but also the liver parenchyma and sometimes encircled hepatocytes. MSC and MSC-CM therapies reversed the increase in the quantitative area occupied by infiltrated BMDCs in liver of HFD- and STZ-vehicle mice (Figs. 3A and 4A, right).

We investigated the population of macrophages, which expressed F4/80 in BMDCs of diabetic liver. Infiltration of BM-derived macrophages (Figs. 3B and 4B, yellow) was remarkably increased in HFD- and STZ-vehicle mice, but was reversed to normal levels by MSC and MSC-CM therapies.

MSC and MSC-CM Therapies Modified the Character of BMDCs Infiltrating Liver and Mononuclear Cells in Peripheral Blood of HFD- and STZ-Diabetic Mice. Expression of interleukin (*Il*)-*6* and *Cd11c*, markers for classically activated macrophages, was unchanged in HFD-vehicle mice, compared to controls, although MSC and MSC-CM therapies down-regulated *Cd11c* expression (Fig. 3C). *Il-6* and *Cd11c* expression was up-regulated in STZ-vehicle mice, but was suppressed by MSC and MSC-CM therapies (Fig. 4C). Expression of *Fizz1* (found in inflammatory zone 1) and *Mrc1* (mannose receptor C type 1), markers for alternatively activated macrophages, was significantly decreased in HFD- and STZ-vehicle mice, compared to controls, but was reversed to normal levels or up-regulated by MSC and MSC-CM therapies (Figs. 3C and 4C).

MSC and MSC-CM Therapies Regulated Interaction Between BMDCs and Endothelial Cells in the Liver. Intracellular adhesion molecule 1 (ICAM-1) was stained in hepatic sinusoidal endothelial cells (HSECs), particularly in the periportal area in controls. Staining intensity was notably increased in HFD- and STZ-vehicle mice, but was decreased to control levels by MSC and MSC-CM therapies (Figs. 3D and 4D). Expression of *Ccr2* (C-C chemokine receptor 2), a receptor for monocyte chemotactic protein (MCP)−1, in GFP-positive BMDCs in the liver was significantly increased in HFD- and STZ-vehicle mice, compared to controls, in which *Ccr2* had been reversed to an almost normal level by MSC and MSC-CM therapies (Figs. 3E and 4E). Furthermore, expression of *Ccr2* in

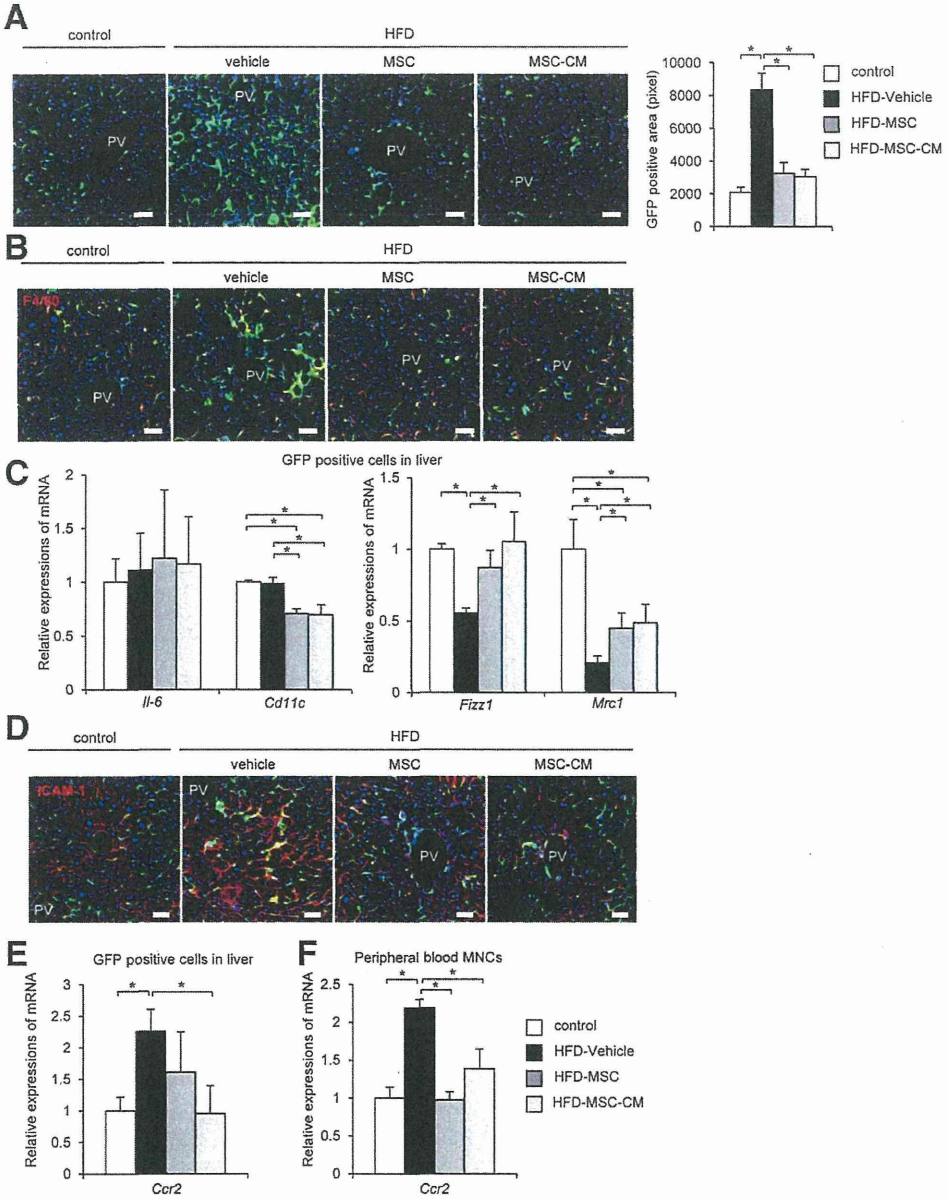

Fig. 3. BMDCs infiltrating liver of GFP-chimeric HFD-diabetic mice. (A) GFP-expressing BMDCs in the liver. GFP-positive density in the liver is quantified in right panel (mean value of 20 panels per group). (B) Immunofluorescence staining of F4/80 (red) in the liver. (C) mRNA expression of *Il-6*, *Cd11c*, *Fizz1*, and *Mrc1* on GFP-positive BMDCs in the liver. (D) Immunofluorescence staining of ICAM-1 (red) in the liver. mRNA expression of *Ccr2* on GFP-positive BMDCs in the liver (E) and PBMCs (F). Relative amounts of mRNA are normalized to an internal control, β-actin. Bar, 50 μm. Data are expressed as mean ± SE values of 5-8 animals. $^*P < 0.05$. mRNA, messenger RNA.

circulating mononuclear cells in peripheral blood of HFD- and STZ-vehicle mice was significantly increased, but MSC and MSC-CM therapies again reversed this increase (Figs. 3F and 4F).

MSC and MSC-CM Therapies Suppressed Proinflammatory Cytokine/Chemokine Expression in Liver of HFD- and STZ-Diabetic Mice. Inflammatory molecules, such as TNFα, MCP-1, and Toll-like receptor 4 (TLR4), were densely stained in both hepatocytes and BMDCs of HFD- and STZ-vehicle mice, and the staining was remarkably decreased by MSC and MSC-CM therapies (Figs. 5A and 6A). Fatty-acid-binding protein 4 (FABP4) was expressed in both sinusoidal endothelial cells (SECs) and hepatocytes of HFD-vehicle mice, and the staining intensity in hepatocytes was decreased by MSC and MSC-CM

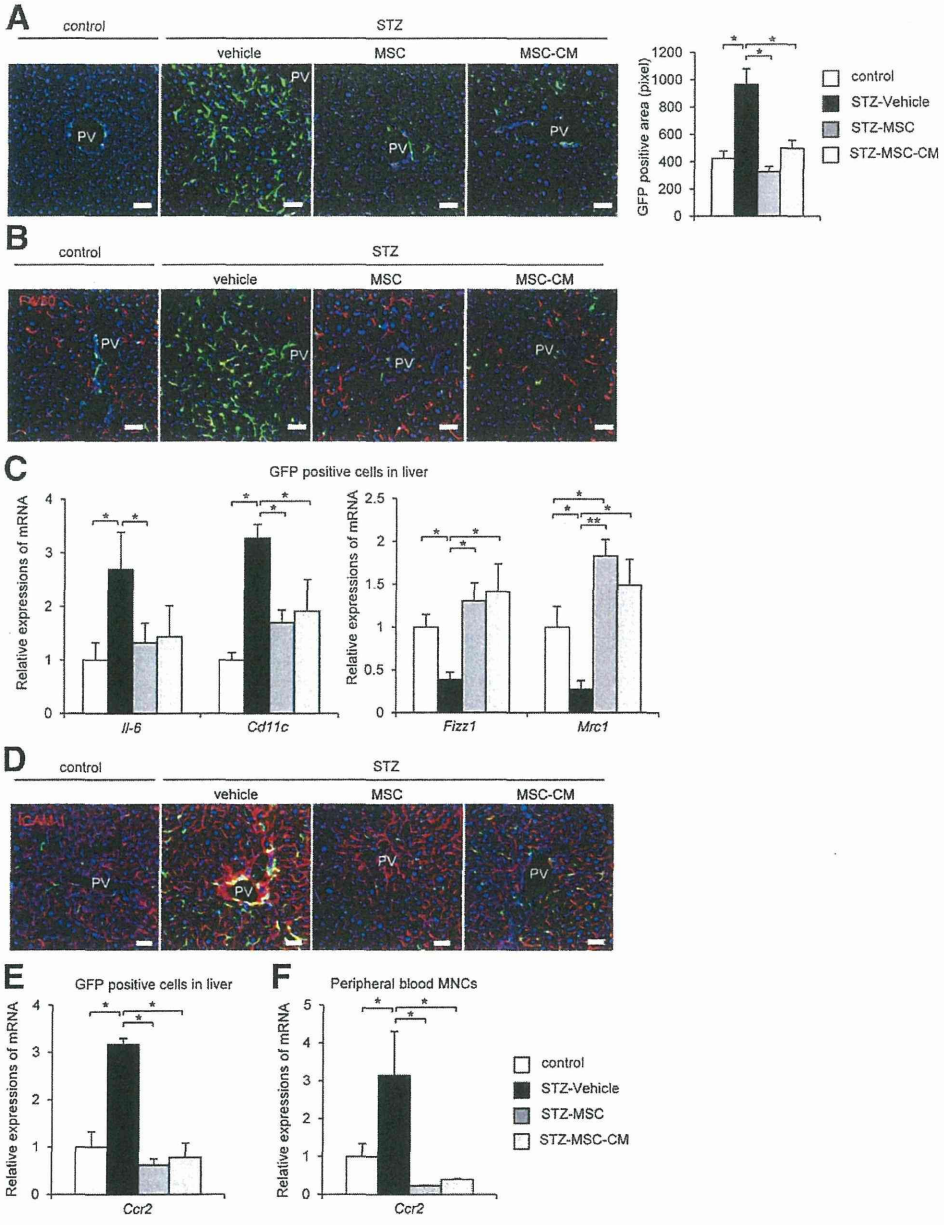

Fig. 4. BMDCs infiltrating liver of GFP-chimeric STZ-diabetic mice. (A) GFP-expressing BMDCs in the liver. GFP-positive density in the liver is quantified in right panel (mean value of 20 panels per group). (B) Immunofluorescence staining of F4/80 (red) in the liver. (C) mRNA expression of *Il-6*, *Cd11c*, *Fizz1*, and *Mrc1* on GFP-positive BMDCs in the liver. (D) Immunofluorescence staining of ICAM-1 (red) in the liver. mRNA expression of *Ccr2* on GFP-positive BMDCs in the liver (E) and PBMCs (F). Relative amounts of mRNA are normalized to an internal control, β-actin. Bar, 50 μm. Data are expressed as mean ± SE values of 5-9 animals. $^*P < 0.05$. mRNA, messenger RNA.

therapies (Fig. 5A). The receptor for advanced glycation endproducts was also densely stained in hepatocytes of STZ-vehicle mice, but staining intensity was decreased by MSC and MSC-CM therapies (Fig. 6A).

MSC and MSC-CM Therapies Regulated Inflammation, Proliferation, and Survival Signaling of Hepatocytes in HFD- and STZ-Diabetic Mice. Phosphorylation of c-Jun amino-terminal kinases (JNKs) and p38 mitogen-activated protein kinase (MAPK) was activated in liver of HFD- and STZ-vehicle mice (Figs. 5B, 6B), whereas activation of extracellular signal-regulated kinase (ERK)1/2 and protein kinase B (Akt) was suppressed in the liver (Figs. 5C and 6C). MSC and MSC-CM therapies reversed these alterations in both HFD- and STZ-diabetic mice.

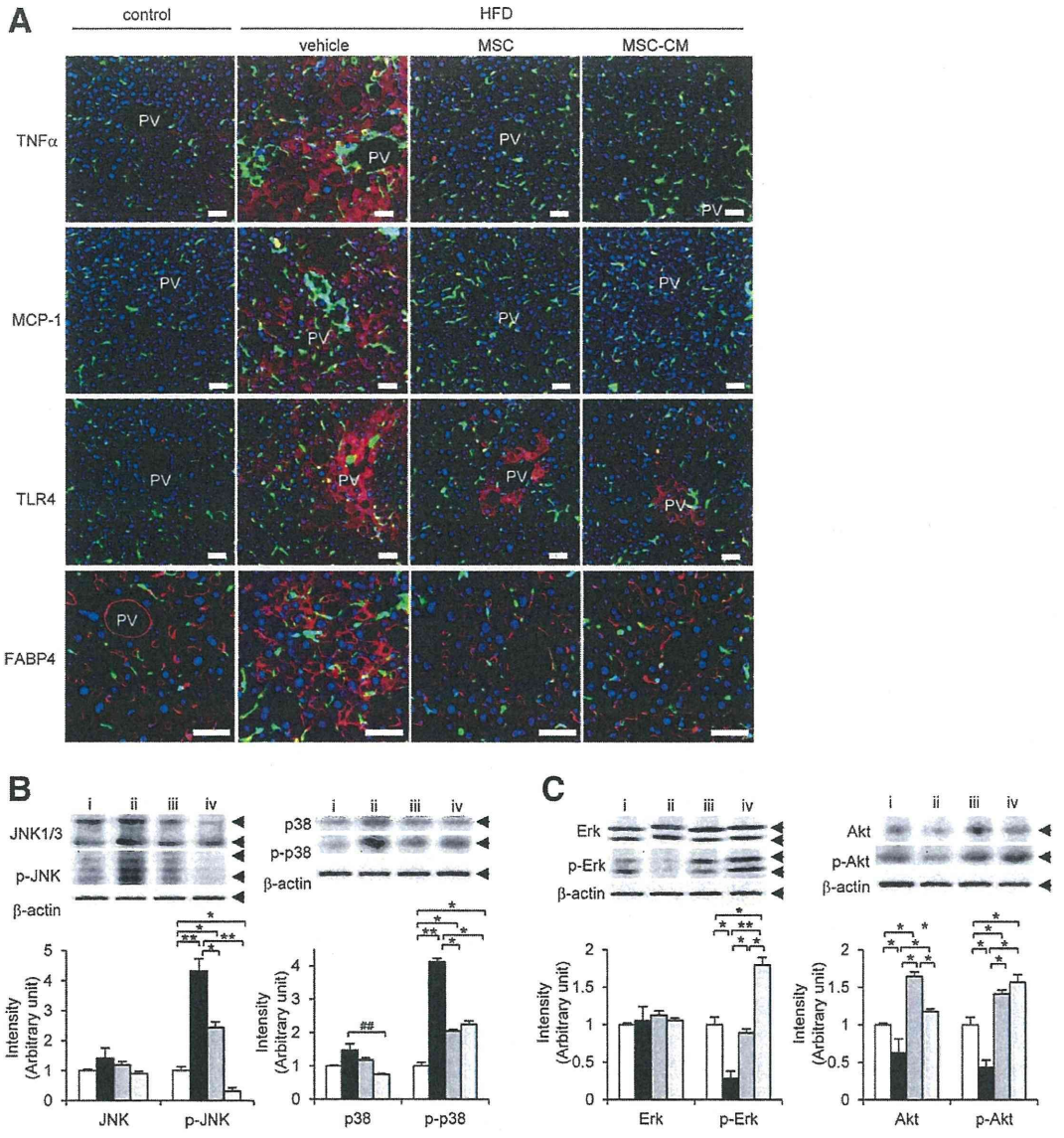

Fig. 5. Anti-inflammatory, proliferative, and antiapoptotic effects of rMSCs and rMSC-CM therapies in liver of HFD-diabetic mice. (A) Immunofluorescence staining (red) of TNFα, MCP-1, TLR4, and FABP4 in the liver. Bar, 50 μm. Protein levels of (B) JNK1/3, phosphorylation of JNK (p-JNK), p38-MAPK, phosphorylation of p38-MAPK (p-p38), (C) Erk1/2, p-Erk, Akt, and p-Akt in liver of mice in each group. (D) Photomicrographs of representative sections of the TUNEL reaction. The apoptotic index is quantified in right panel (mean value of 20 panels per group). (E) Protein levels of Bax, Bcl2, caspase-3, and cleaved caspase-3 in liver of mice in each group. Relative amounts of protein are normalized to an internal control, β-actin. Intensity is shown as an arbitrary unit (n = 5, each group). Data are expressed as mean ± SE values $*P < 0.05$; $**P < 0.01$.

MSC and MSC-CM Therapies Suppressed Apoptosis of Hepatocytes in HFD-Diabetic Mice and Enhanced Regeneration of Damaged Hepatocytes in STZ-Diabetic Mice. MSC and MSC-CM therapies markedly decreased terminal deoxynucleotidyl transferase-mediated dUTP nick end labeling (TUNEL)-positive cells in liver of HFD-diabetic mice (Fig. 5D). Mitochondria control cell fate by apoptosis-related molecules, such as Bax and B-cell lymphoma 2 (Bcl2), and the subsequent activation of caspase-3. The results showed that expression of Bax and cleaved caspase-3 was significantly increased in liver of HFD-vehicle mice. In addition, Bcl2 expression was significantly decreased in liver of HFD-vehicle mice. These alterations were reversed by MSC and MSC-CM therapies (Fig. 5E). On the other hand, expression of hepatocyte nuclear factor 4 (HNF-4) was stimulated, and the transcription factor, CCAAT/enhancer-binding protein alpha (C/EBPα), which was down-regulated in STZ-vehicle mice, was notably enhanced or recovered

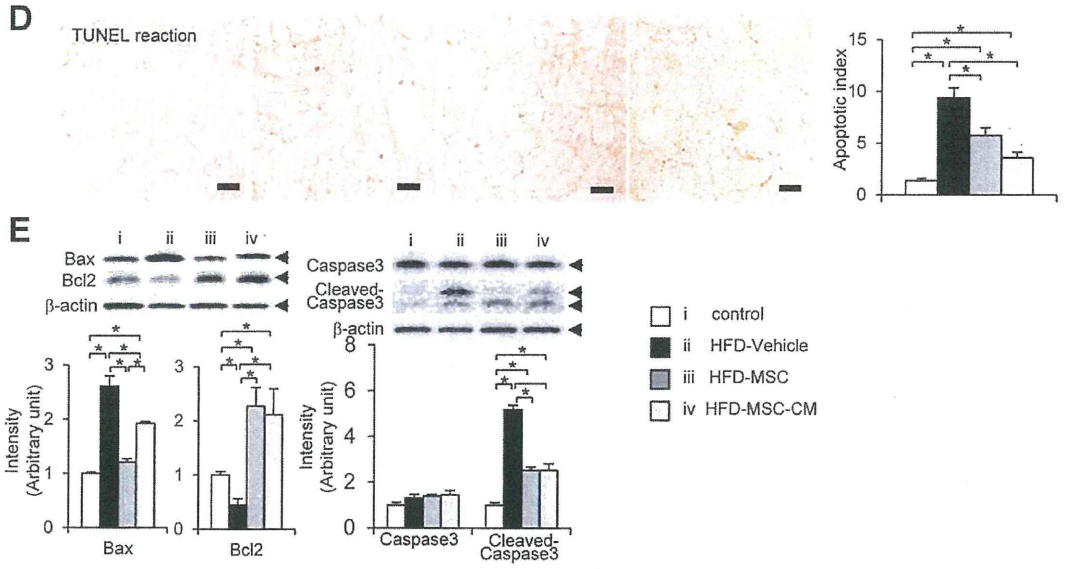

Fig. 5. (Continued)

by MSC and MSC-CM therapies (Fig. 6D). Expression of trophoblast cell-surface antigen 2 (also known as *Trop2*), which was remarkably decreased in STZ-vehicle mice, was recovered by MSC and MSC-CM therapies (Fig. 6E).

MSC and MSC-CM Therapies Prevented Lipogenesis, Fibrosis, Glucogenesis, and IR in Liver of HFD-Diabetic Mice. In HFD-vehicle mice, a number of large lipid droplets were precipitated in hepatocytes, but were decreased in both size and number in HFD-MSC and HFD-MSC-CM mice (Fig. 7A, top). Examination of Azan-stained sections revealed periportal fibrosis in HFD-vehicle mice (Fig. 7A, middle), which was suppressed by MSC and MSC-CM therapies. Expression of transforming growth factor beta 1 (TGF-β1), a marker of stellate cells, was increased in both resident cells and BMDCs in liver of HFD-vehicle mice, but was recovered by MSC and MSC-CM therapies (Fig. 7A, bottom).

Phosphorylation of insulin receptor substrate 2 (p-Irs2) serine and sterol response element-binding protein 1c (SREBP-1c) levels was notably up-regulated in HFD-vehicle mice (Fig. 7B,C) and was completely normalized by MSC and MSC-CM therapies. Beneficent transcriptional activity by forkhead box O1 (FoxO1) was suppressed in liver of HFD-vehicle mice and normalized by MSC and MSC-CM therapies (Fig. 7D). On the other hand, neither total cholesterol nor triglyceride levels were altered by MSC and MSC-CM therapies (Supporting Fig. 2A).

Resistin was densely stained in liver of HFD-vehicle mice and was reduced by MSC and MSC-CM therapies (Fig. 7E, top). Glucose transporter 2 (GLUT2) staining in the liver was reduced in liver of HFD-vehicle mice, but was recovered by MSC and MSC-CM therapies (Fig. 7E, bottom).

We also examined effects of MSC and MSC-CM therapies on serum adiponectin, insulin, and homeostasis model assessment-estimated IR (HOMA-IR) as major factors of IR. Serum adiponectin level was decreased in HFD-vehicle mice and normalized by MSC and MSC-CM therapies (Supporting Fig. 2B). The HOMA-IR level in the liver was significantly increased in HFD-vehicle mice and significantly reduced by MSC and MSC-CM therapies (Supporting Fig. 2B).

Discussion

We investigated the mechanism of action of MSC therapy for different pathological conditions in liver of HFD- and STZ-induced diabetic mice. Because only a limited number of donor MSCs were observed in the liver, we considered that the effects of the administered MSCs on damaged hepatocytes was a result of the humoral factors released from the MSCs. MSC-CM is a cocktail of various trophic factor secreted from MSCs. The present results show that the curative effects of the MSC and MSC-CM therapies on damaged hepatocytes in diabetic mice were similar: Both therapies ameliorated liver dysfunction and IR.

In previous studies reporting on effects of MSCs on hepatocyte damage, blood-glucose levels were recovered by pancreatic β-cell regeneration,[6,7] suggesting that

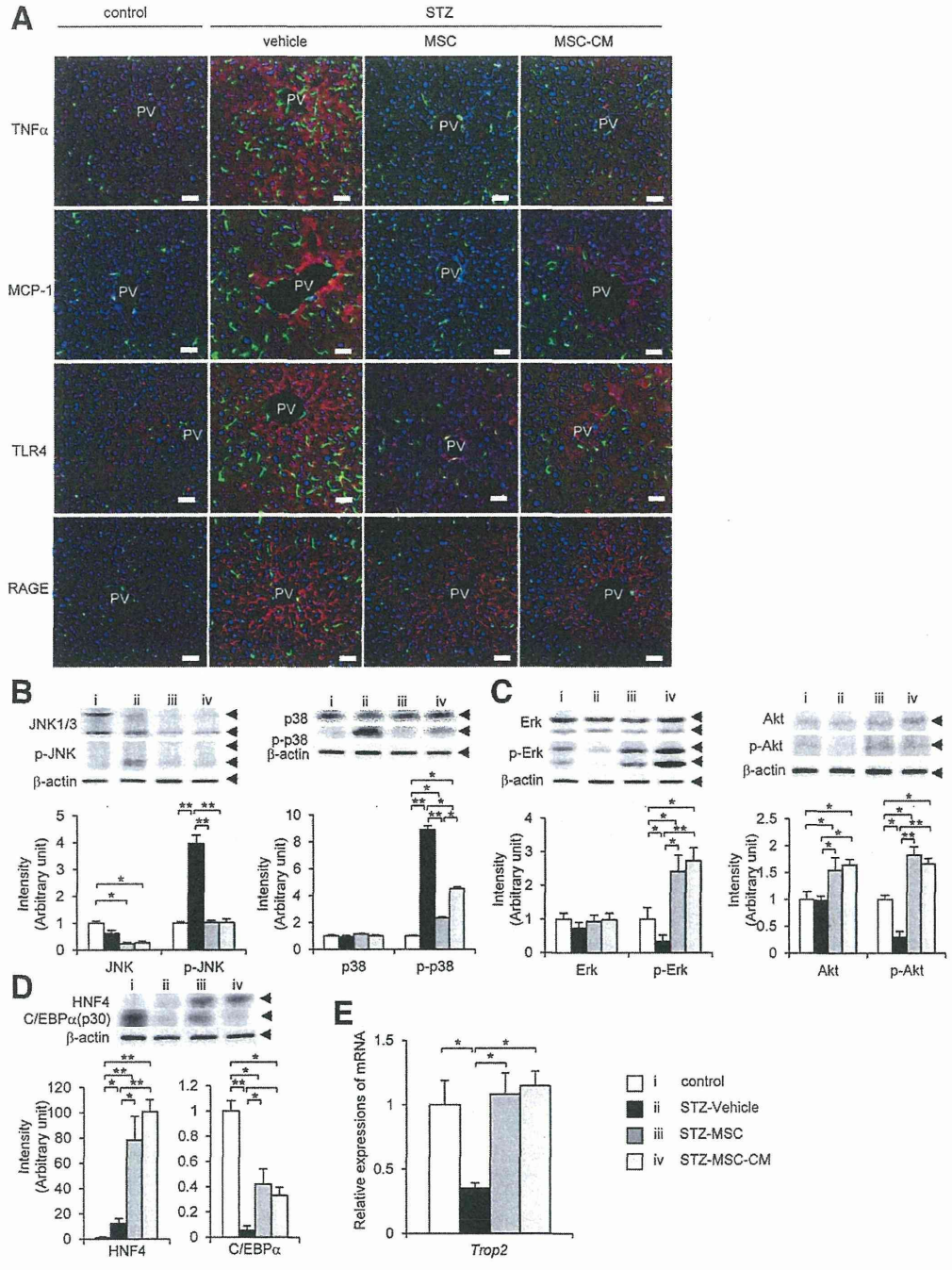

Fig. 6. Anti-inflammatory and proliferative effects and regenerative action of rMSCs and rMSC-CM therapies in liver of STZ-diabetic mice. (A) Immunofluorescence staining (red) of TNFα, MCP-1, TLR4, and receptor for advanced glycation endproducts (RAGE) in the liver. Bar, 50 μm. Protein levels of (B) JNK1/3, p-JNK, p38, p-p38, (C) Erk1/2, p-Erk, Akt, p-Akt, (D) HNF-4, and C/EBPα in liver of mice in each group. Relative amounts of protein are normalized to an internal control, β-actin. Intensity is shown as an arbitrary unit (n = 5, each group). (E) mRNA expression of *Trop2* in liver of each group (n = 5, each group). Relative amounts of mRNA are normalized to an internal control, β-actin. Data are expressed as mean ± SE values. $*P < 0.05$; $**P < 0.01$. mRNA, messenger RNA.

amelioration of hyperglycemia improves liver dysfunction. The present study revealed that even though hyperglycemia did not recover, diabetes-induced liver dysfunction was remarkably reversed by the MSC and MSC-CM therapies. The most interesting point was that hepatocyte regeneration occurred in the STZ-diabetic liver under persistent hyperglycemic conditions.

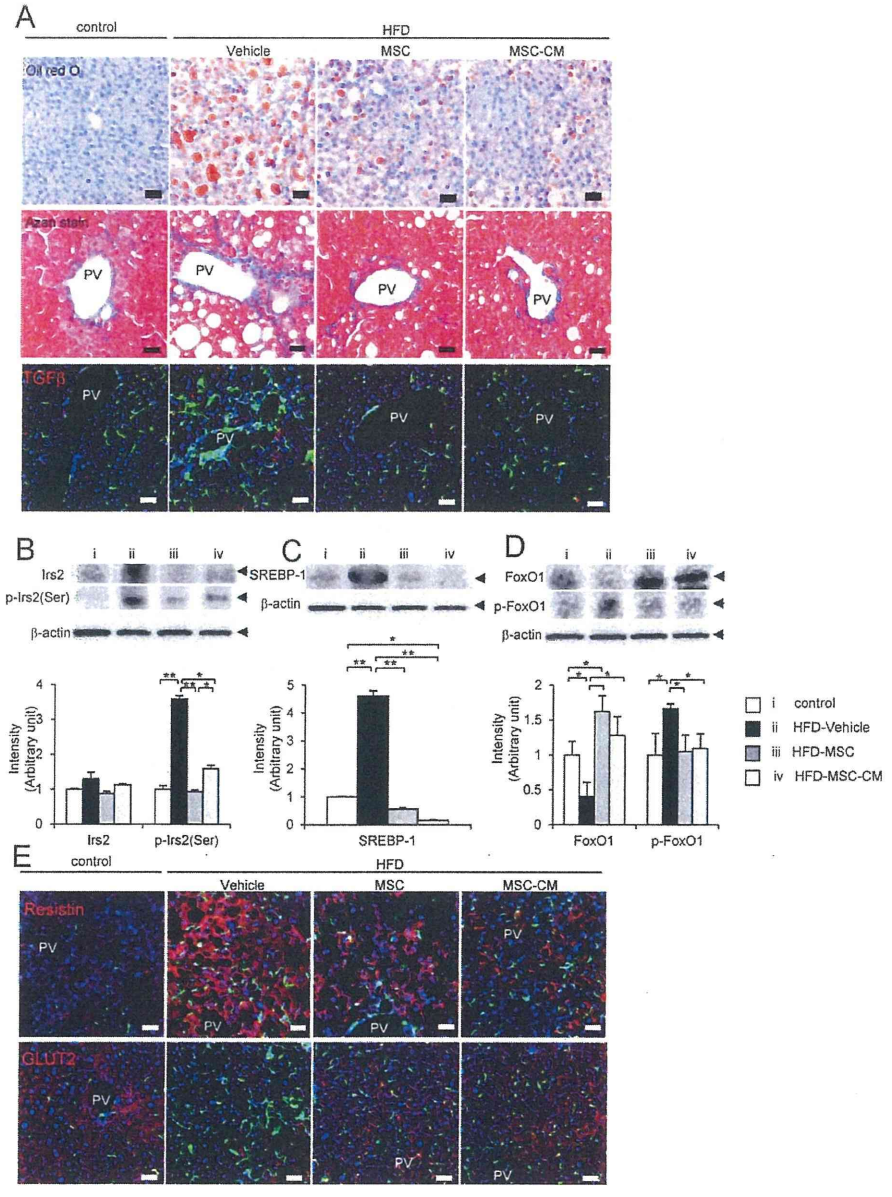

Fig. 7. Effects of rMSC and rMSC-CM therapies on lipogenesis, fibrosis, glucogenesis, and IR of liver in HFD-diabetic mice. (A) Oil Red O staining (top), Azan staining (middle), and TGF-β1 staining (bottom) in liver 8 weeks after initial treatment of MSC and MSC-CM. Lipid droplets are stained red and fibrosis are stained blue. Bar, 50 μm. Protein levels of (B) Irs2, abnormal phosphorylation of Irs2 serine^{723} (p-Irs2), (C) SREBP-1, (D) FoxO1, and phosphorylated FoxO1 (p-FoxO1) in liver of each group. Relative amounts of protein are normalized to an internal control, β-actin. Intensity is shown as an arbitrary unit (n = 5, each group). (E) Immunofluorescence staining (red) of resistin and GLUT2 in liver of each group. Bar, 50 μm. Data are expressed as mean ± SE values. $*P < 0.05$; $**P < 0.01$.

The present results showed a significant increase in BMDC infiltration into liver of HFD- and STZ-induced diabetic mice, which was completely reversed by the MSC and MSC-CM therapies. Macrophages are classified as classically activated macrophages (M1 macrophages) or as alternatively activated macrophages (M2 macrophages).[14] In this study, BMDCs in liver of diabetic mice displayed a molecular profile similar to that of proinflammatory M1 macrophages by expressing *Il-6* and *Cd11c*; however, they changed into M2 macrophages expressing *Fizz1* and *Mrc1* after application of the MSC and MSC-CM therapies. Further changes, including *Ccr2* expression, were also demonstrated in BMDCs in the liver and in mononuclear cells in the peripheral circulation. Expression of MCP-1 was stimulated in liver of diabetic mice, but was remarkably decreased by both therapies, suggesting that accelerated infiltration of BMDCs into the liver induced by MCP-1/CCR2 interactions was blocked by these treatments. ICAM-1 is induced in HSECs by cytokine or chemokine signals and enhances recruitment of inflammatory cells from vessels.[15] Here, notable expression of ICAM-1 in SECs contributed to excessive infiltration of BMDCs and was also suppressed by the MSC and MSC-CM therapies.

The present findings showed that both the MSC and MSC-CM therapies ameliorated inflammatory change and apoptotic reactions in hepatocytes caused